Composite action on web post buckling shear resistance of composite cellular beams with PCHCS and PCHCSCT

Felipe Piana Vendramell Ferreira*[a], Konstantinos Daniel Tsavdaridis[b], Carlos Humberto Martins[c], Silvana De Nardin[a]

[a]Department of Civil Engineering, Federal University of São Carlos, Rod. Washington Luiz, km 235, São Carlos, São Paulo, Brazil.

[b]School of Civil Engineering, Faculty of Engineering and Physical Sciences, University of Leeds, Woodhouse Lane, LS2 9JT Leeds, UK.

[c]Department of Civil Engineering, State University of Maringá, Av. Colombo nº 5790, Maringá, Paraná, Brazil.

*Corresponding author

E-mail address: fpiana@live.com (F. P. V. Ferreira), K.Tsavdaridis@leeds.ac.uk (K. D. Tsavdaridis), chmartins@uem.br (C. H. Martins), snardin@ufscar.br (S. De Nardin)

Abstract

This paper aims to study the composite action on web post buckling (WPB) resistance of composite cellular beams with precast hollow core slab (PCHCS) units and with precast hollow core slab units with concrete topping (PCHCSCT). Geometrical and material non-linear analyses are performed. A parametric study is developed, varying the opening diameter, the web post width and the shear studs spacing, with single and double row. It was found that the models with double row of shear studs showed global shear resistance greater than or equal to the models with only one row. For models with PCHCS, in some analyses there was a reduction in global shear resistance due to the absence of shear studs in the second opening, close to the support. For PCHCSCT models, there was an increase in the global shear resistance, in comparison with PCHCS models. However, in most of these models, the shear stud rupture occurred. Finally, the WPB models were compared with a simplified equation that take into account the global shear resistance due to buckling, composite action and Vierendeel bending. The average, standard deviation and variation value of the ratio between the analytical and numerical models were 0.833, 12.47% and 1.55%, respectively.

Keywords: Shear studs; Cellular beams; Precast hollow core slabs; Global shear force; Geometrical nonlinear analyses.

NOTATION

The following symbols are used in this paper:

CT Concrete Topping

PCHCS Precast hollow core slab

PCHCSCT Precast hollow core slab with concrete topping

VM Vierendeel mechanism

*VM** Vierendeel mechanism combined with shear stud rupture

WPB+PM Web post buckling combined with plastic mechanism

*WPB+PM** Web post buckling combined with plastic mechanism and shear stud rupture

A_T the area of the tee

A_{wT} the web area of the tee

b_f the width of the flange

b_w the width of the web post

b_{we} the width of the end post

C the axial compressive resistance of slab;

D_o the opening diameter

d the depth of parent section;

d_{sc} the diameter of shear stud;

d_g the depth of cellular beam

f_c the concrete compressive cylinder strength

$f_{cr,w}$ the buckling stress acting across the web-post

f_t the concrete tension strength

f_u the ultimate strength of cellular beam

f_y the yield strength of cellular beam

g gap (transverse distance between slab panels)

h_c the depth of concrete above decking profile

h_{eff} the effective depth of cellular section between centroids of the tees

h_s the total depth of slab

K_c the ratio of the second stress invariant on the tensile meridian to that on the compressive meridian, $0.5 \le K_c \le 1.0$

k the number of shear stud rows

L the length of composite cellular beam

L_e the distance between points of zero bending

l_o the opening length

l_{eff} the effective length of web-post

n the number of shear studs for $L/2$

n_f the number of shear studs for full shear connection

P_{sc} the resistance of shear stud

p the length between the opening diameter centers

s the shear stud spacing

t_f the thickness of the flange

t_w the thickness of the web

V the global shear force

$V_{pl,T}$ the plastic shear resistance of tee

V_{VC} the shear resistance due to composite action

V_{WPB} the web post buckling shear resistance

z_{pl} the depth of the plastic neutral axis of tee from outer face of flange

y_t the depth of the geometric axis of tee from outer face of flange

β_c the dimensionless constant in Eqs. (1-2)

ε strain

ε_c the compressive strain

ε_t the tensile strain

η $2n/n_f$

λ_0 the reduced slenderness factor

λ_w the web slenderness ratio

μ the viscosity parameter that represents the relaxation time

ξ the eccentricity (defines the rate at which the function approaches the asymptote, the default value is 0.1)

σ stress

σ_{b0} the initial equibiaxial compressive yield stress

σ_{c0} the initial uniaxial compressive yield stress

χ the reduction factor

Ψ the dilation angle

1. INTRODUCTION

Cellular beams are manufactured from a parent section that goes through the processes of thermal cutting, expansion and welding (**Fig. 1**). The result of manufacture is a beam with expanded section and periodical circular web openings. The cross-section expansion provides greater flexural stiffness, and the presence of openings favors air flow in closed environments as well as the passage of ducts for the integration of services. The composite cellular beams are able to span between 12m and 20m [1,2]. Solid or composite slabs have disadvantages, such as the high operational cost of welding the shear studs, and the curing time. Thus, to reduce some of these limitations, the use of PCHCS is an alternative [3]. Generally, in the construction buildings with PCHCS, a concrete topping (CT) is made to provide a smooth and uniform finish. The CT is 40 to 100 mm thick, of strength between 25 and 40 MPa, and a small amount of reinforcement to control the shrinkage [4,5].

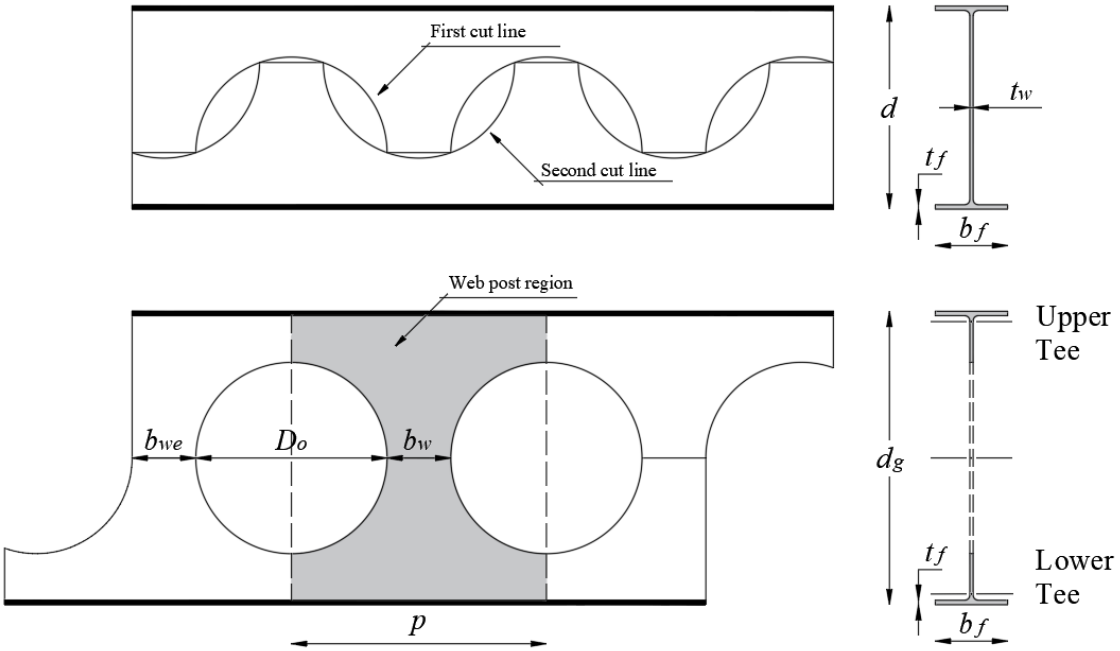

Fig. 1: Cellular beams manufacturing process [6]

The resistance of composite cellular beams is governed by slab failure modes, such as cracking or crushing, with cellular beam failure modes, such as web post buckling (WPB) and Vierendeel mechanism (VM) [6]. The WPB becomes critical when the web post width is reduced [7]. This phenomenon is characterized by a lateral displacement with torsion at the web post. The WPB resistance depends on geometric characteristics of the cellular beam, such as the opening diameter, the web post width and the web thickness [7–11]. The VM occurs when the tees reach the yield strength due to the combination of normal and tangential stresses. It is a phenomenon characterized by the distortion and formation of plastic hinges in regions close to the opening [11–13]. In the case of composite cellular beams, the main parameters that affect this structural behavior are the web thickness, the opening diameter, and the number of shear studs above the critical opening length (l_o) (**Fig. 2**), which is known as local composite action between the upper tee and slab [1,11,14]. For cellular beams, the critical opening length is equal $0.45D_o$ [1,15]. The shear studs are the mechanical devices most commonly used in construction. This is due to its flexible behavior, which allows slipping between the concrete slab and the steel profile before reaching the failure [16].

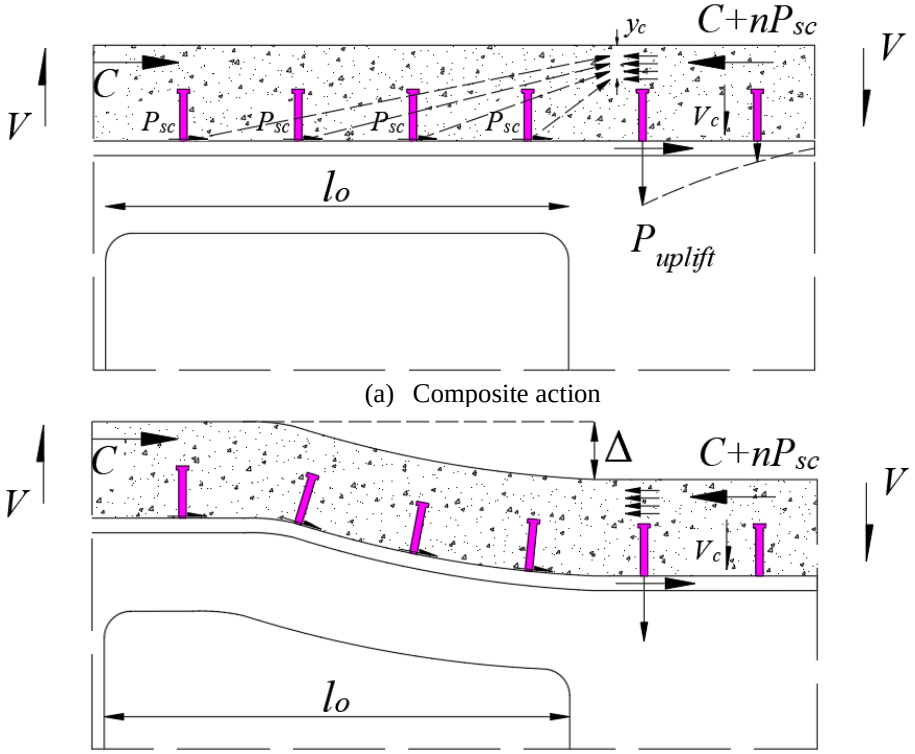

(a) Composite action

(b) Effects of flexibility at a long opening.

Fig. 2: Composite action of upper tee and slab, adapted from [1]

On the calculation and design of composite cellular beams, there are currently two recommendations: SCI P355 [15] and Steel Design Guide 31 [17], which are based on EC4 [18] and ANSI/AISC 360-16 [19], respectively. Both publications are aimed in composite cellular beams with steel-concrete composite slabs, condition in which the shear stud positions are limited by the position of the rib. The SCI P355 [15] recommendations considers the influence of shear studs in checking the bending (full or partial interaction), and in the VM resistance, as shown in **Fig. 2**. On the other hand, the Steel Design Guide 31 [17] considers the shear studs in checking the bending. Another project recommendations on cellular beams was presented by the Centre Technique Industriel de la Construction Métallique (CTICM) [20–22], and it is based on EC3 [23]. These calculation procedures were introduced in the ACB+ software for ArcelorMittal [24]. Verweij [21] described that the method is the most advanced[1], however, the coefficients for calculating the critical forces in the web-post are not available because they are property of ArcelorMittal.

There are studies in the literature that investigated the influence of the shear studs allocated above the opening length in composite beams with web openings [25–29]. However, such studies focused on composite beams with a single rectangular web opening, which is a different structural system from that with periodical web openings, as is the case with composite cellular beams (**Fig. 1**). In addition, the previous studies addressed only steel-concrete composite slabs. Ferreira et al. [30] developed a finite element model of composite cellular beams with PCHCS and PCHCSCT. However, the influence of composite action on resistance has not been investigated. This paper aims to study the shear studs spacing on global shear resistance of composite cellular beams with PCHCS and PCHCSCT. A numerical model is developed using the finite element method. A parametric study is carried out, varying the key parameters of the cellular beams, such as the web-post width and the opening diameter, as well as the spacing

[1] The method was based on a series of tests and numerical modeling.

between the shear studs in 150mm, 300mm and 450mm, with a single and double row. 240 geometrical and material non-linear analyses are performed. The composite action is studied, and the global shear force that causes the WPB is investigated as a function of spacing and the number of shear studs. The results are discussed, according to the parameters studied.

2. BACKGROUND

The studies of the flexural behavior of composite beams with PCHCS started with Lam [31]. Later, several studies were published by the author [32–36]. Lam et al. [35] presented four-point bending results of composite beams with PCHCS. The authors observed the ductile failure, which can be controlled by the appropriate use of transverse reinforcement. Lam et al. [36] complemented the previous study with parametric finite element analyses. The numerical modeling results allowed the determination of the effective width of the PCHCS. Until then, no results had been published on the influence of the shear studs, the infill concrete and the gap (g), which is the distance between the slab panels, on the flexural behavior. Ellobody and Lam [32] investigated such parameters with pushout tests. The authors observed that the resistance of the shear stud increased with the increase of the gap, for the transverse reinforcement diameter less than 16 mm. However, this increase was observed for gap widths of up to 80 mm. Lam [33] presented pushout tests, in order to investigate the influence of the slab cutting angle (chamfered or squared), the transverse reinforcement rate and the shear stud diameter. Transverse reinforcements were the dominant factor affecting the force-slip relationship. In 2003, the Steel Construction Institute (SCI) published the SCI P287 [37], which was a manual containing design recommendations for composite beams with PCHCS. Subsequently, the SCI P401 [38], an update of the previous document, was published. The updated document collects recommendations of minimum dimensions, considering the ultimate and service limit states in the construction phase for cases of full and partial interaction.

In view of the concrete topping influence, Baran [4] investigated the flexural behavior of PCHCSCT. The results showed improvements in the cracking moment, and in the initial stiffness of the PCHCS. Ibrahim et al. [5] conducted an experimental study of the shear-bending resistance of PCHCSCT. The authors observed that the ideal condition for the interface between the PCHCS and CT, aiming greater stiffness and resistance to shear, was the rough and wet. Araújo et al. [16] investigated the behavior of shear studs in composite beams with PCHCSCT by pushout tests. According to the authors, there were some changes in the resistance of each connector due to the presence of the CT. Batista and Landesmann [39] tested composite beams with PCHCSCT by four-point bending. The results showed similar collapse mode, i.e. the cracks propagated along the width of the PCHCSCT, extending from the side face of the slab to the region of connection with the steel profile; a factor that caused the stiffness of the composite beam to be reduced. Ferreira et al. [40] conducted a parametric study in composite beams with PCHCS and PCHCSCT. The authors concluded that the CT increased the initial stiffness of the composite beams, as well as its resistance, according to [4,5]. From the background exposed so far, it appears that studies of composite beams with PCHCS and PCHCSCT are quite recent.

The initial studies involving composite beams with web openings examined beams with a single rectangular opening formed by solid [41–48] or composite slabs [25–29,49–55]. Several studies have investigated the behavior of the steel-concrete interface as a function of the shear studs. Regarding the composite beams with rectangular web opening and solid slab, Todd and

Cooper [46] presented a calculation methodology to estimate the resistance of composite beams considering full interaction between steel-concrete interface. The authors' model underestimated the resistance of composite beams with rectangular web opening, when compared with Granade's tests results [41]. In Narayanan et al. [44], the shear resistance of composite girders with web rectangular openings was investigated. The results showed that if there is an adequate connection at the steel-concrete interface, the shear resistance of the composite girders with rectangular web openings would considerably increase the resistance of the composite action.

In the matter of the composite beams with rectangular web openings and composite slabs (with trapezoidal steel formwork), Redwood and Poumbouras [25] studied the need for shear studs, in the steel-concrete interface, allocated in the opening length. It was found that the absence of shear studs in the opening length significantly reduced the resistance of the composite beam with rectangular web openings. Subsequently, Redwood and Poumbouras [26] presented a model for the calculation of the resistance, considering the increase in compression stresses due to the slip caused by the deformation of the shear studs. Such methodology was shown to be conservative when compared to previous experimental results [25]. Donahey and Darwin [27] investigated the effects of the moment-shear ratio, quantity and position of the shear studs, orientation and position of the steel formwork. The results showed that when the number of connectors was increased above the opening, the resistance of the composite action was also increased. Cho and Redwood [28] presented a methodology capable of estimating the resistance of composite beams with rectangular web openings, considering the shear studs above the opening region as tensioned elements. This methodology was based on the truss concept. According to the authors, the basic concept of this analogy was that after cracking, the concrete carried a set of compression stresses in diagonals and the reinforcement tensile stresses. This approach related the shear resistance to the location of the shear studs. Subsequently, Cho and Redwood [29] found through tests that the shear studs positioned in the opening length were responsible for the contribution of the concrete slab in the shear resistance. It has been observed so far, that the studies which addressed the position of the shear studs considered only the composite beams with rectangular web openings. More information about these previous studies can be found in Ferreira et al. [56].

Regarding studies of composite cellular beams with periodical circular openings web openings (**Fig. 1**), Müller et al. [57] presented tests and parametric studies. According to the authors, the resistance of the cellular beam was preponderant, since the failure was achieved by the WPB. The models presented by Nadjai [58] and Nadjai et al. [59] had the ultimate resistance governed by the WPB; a conclusion similar to the models of Müller et al. [57]. Sheehan et al. [60] tested composite cellular beams with long spans. The authors observed that the composite cellular beams resisted 3.4 times the estimated design load, despite the interaction degree is considerably less than the minimum required by EC4 [18]. EC4 makes [18] recommendations on the minimum interaction degree for composite beams with spans less than 25m, considering symmetrical (**Eq. 1**) and asymmetric (**Eq. 2**) steel sections:

$$\eta \geq 1 - \left(\frac{355}{f_y}\right)\left(0.75 - 0.03L_e\right), \quad \eta \geq 0.4 \tag{1}$$

$$\eta \geq 1-\left(\frac{355}{f_y}\right)\left(0.3-0.015L_e\right), \quad \eta \geq 0.4 \tag{2}$$

Ferreira et al. [6] investigated the WPB resistance of composite cellular beams and verified the influence of the composite slab and the end-post width (b_{we}) on the resistance. The authors concluded that the existing procedures underestimate the WPB resistance. Ferreira et al. [61] complemented the previous study, considering buckling and post-buckling analyses. The authors verified the modes of deformation of the composite cellular beams, and concluded that for asymmetric sections, the web post buckling can be characterized by the formation of a C-shaped buckling curvature. Ferreira et al. [30] presented a finite element model which is capable of predicting the resistance of composite cellular beams with PCHCS and PCHCSCT. In this study, the resistance of composite cellular beams with PCHCS and PCHCSCT was compared with the resistance of composite cellular beams with composite slabs. According to the authors, the models with PCHCS and PCHCST showed greater resistance. Consequently, there are no yet studies that have investigated the influence of the shear studs positioning on the shear resistance of composite cellular beams with PCHCS and PCHCSCT.

3. FINITE ELEMENT MODEL: VALIDATION STUDY

In the present study is used the same numerical model that was developed and validated by Ferreira et al. [30]. Therefore, in this section the validation results are presented briefly. More information regarding the validation study can be found in [30]. The experimental studies and the validation results are presented in **Table 1** and **Fig. 3**, respectively.

Table 1: Models (in mm, MPa and GPa) [30]

Model	Ref	d or d_g	D_o	p	Upper tee					Lower tee				
					b_f	t_f	t_w	f_y (flange/web)	f_u (flange/web)	b_f	t_f	t_w	f_y (flange/web)	f_u (flange/web)
CCB1	[58]	575	375	500	141.8	8.6	6.4	312	438.5	141.8	8.6	6.4	312	438.5
CCB2	[58]	630	450	630	141.8	8.6	6.4	312	438.5	152.4	10.9	7.6	312	438.5
CCB3	[57]	555	380	570	180	13.5	8.6	451/489	541/587	180	13.5	8.6	451/489	541/587
CCB4	[57]	485	380	570	150	10.7	7.1	407/467	524/588	300	21.5	12	453/488	519/582
CB1	[62]	355	-	-	171.5	11.5	7.4	310/355	$1.3f_y$	171.5	11.5	7.4	310/355	$1.3f_y$
CB2	[62]	355	-	-	171.5	11.5	7.4	310/355	$1.3f_y$	171.5	11.5	7.4	310/355	$1.3f_y$
CB3	[39]	299	-	-	306	11	11	345	450	306	11	11	345	450

Model	Ref	Slab		Reinforcement		b	L	L_p
		f_c	$f_{c,PCHCS}$	φ	f_s			
CCB1	[58]	28.6	-	-	-	1200	4500	1750
CCB2	[58]	28.6	-	-	-	1200	4500	2250
CCB3	[57]	33.6	-	-	-	1800	6840*	1140/2850
CCB4	[57]	24.0	-	-	-	1800	6840*	1140/2850
CB1	[62]	25.6	40	16	585	1665	5700	1500
CB2	[62]	20.8	40	8	473	1665	5700	1500
CB3	[39]	30.0	45	12.5	500	1756	5830	1915

*Slab cut back by 285 mm at end of cellular beam

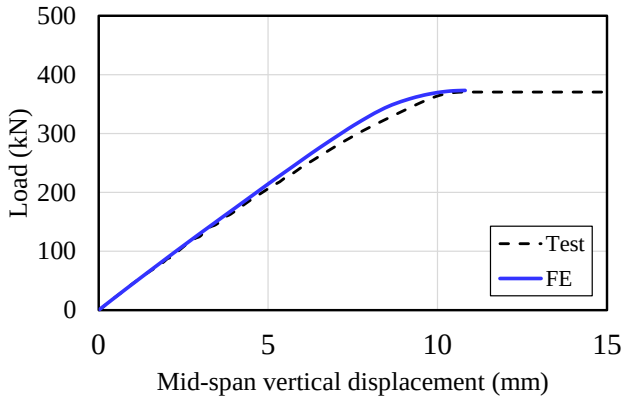

(a) CCB1

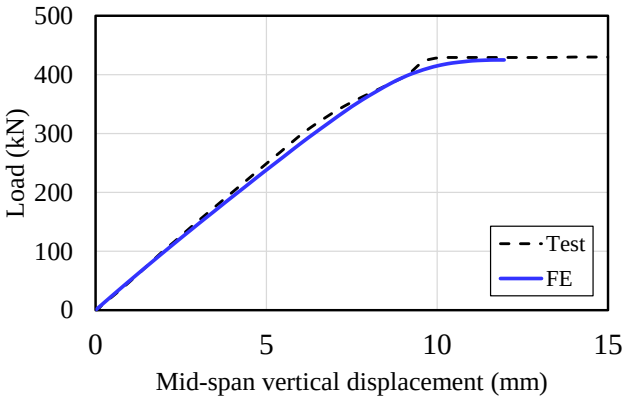

(b) CCB2

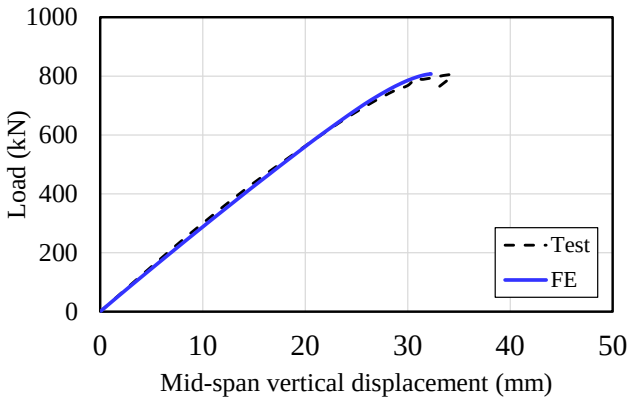

(c) CCB3

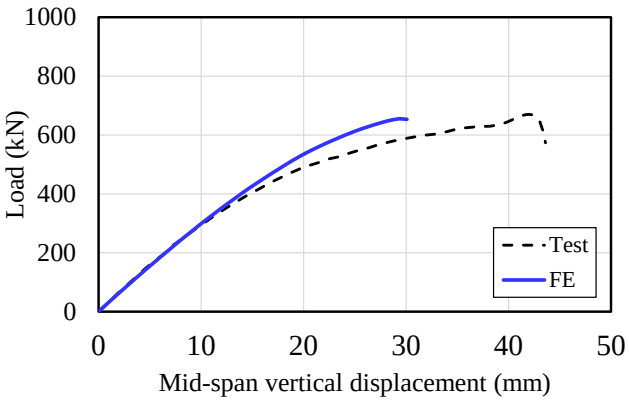

(d) CCB4

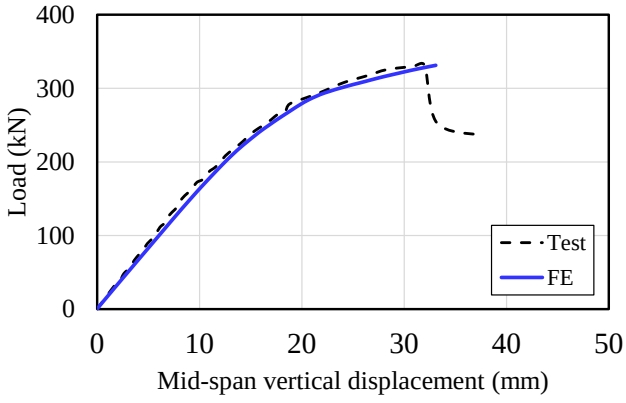

(e) CB1

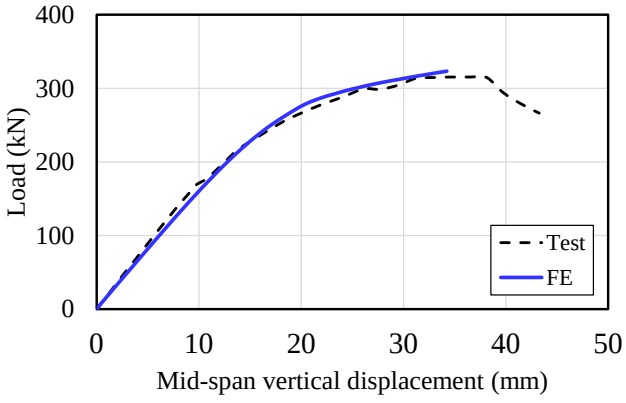

(f) CB2

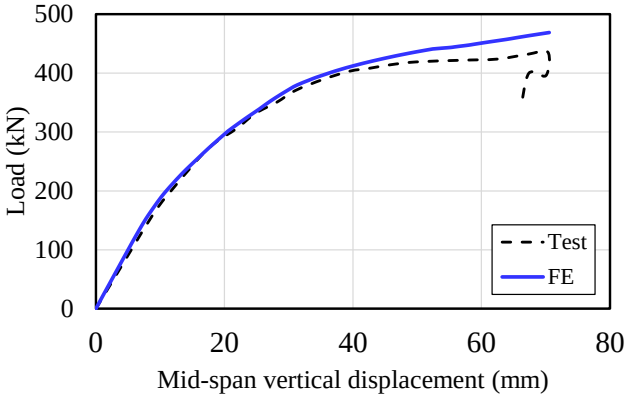

(g) CB3

153 **Fig. 3: Validation results** [30]

4. FINITE ELEMENT MODEL: PARAMETRIC STUDY

The general considerations of the parametric study are presented in this section, as well as the type of analyses, the constitutive materials models, the interaction between the contact surfaces, the boundary conditions and discretization. The following are the general considerations for the parametric study:

1. The yield stress and the ultimate stress of the shear stud are 460 MPa and 559 MPa, respectively. The elongation at rupture is 18.8%;
2. The W360x91 profile is considered as parent section. The total height of the cellular section (d_g) is 530mm;
3. The ASTM A572 Grade 50 steel is adopted (f_y=345 MPa and f_u=450 MPa). The Young's modulus is 200 GPa;
4. The ratio p/D_o is varied in 1.2, 1.3, 1.4 and 1.5, and the ratio D_o/d is varied in 0.8, 0.9, 1.0, 1.1 and 1.2;
5. For PCHCS LP15 units (**Fig 4**) is considered. The filling of the 1st, 3rd, 5th and 7th core is considered, and a transversal reinforcement with 16mm of diameter is placed;

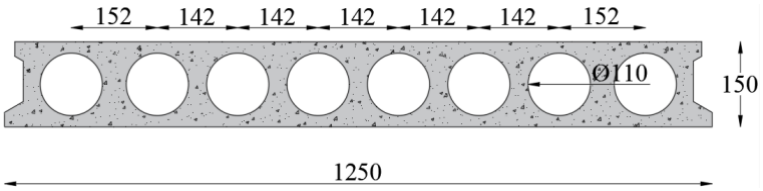

Fig. 4: LP 15

6. For PCHCS, 130mm of gap is considered;
7. The thickness of CT is 50mm, and a steel mesh is 4.2mm spaced at 100mm;
8. The shear stud dimension is 19x125mm. One and two rows of shear studs are considered, varying the longitudinal spacing in 150mm, 300mm and 450mm (**Fig.5**). The transversal spacing is $4d_{sc}$.

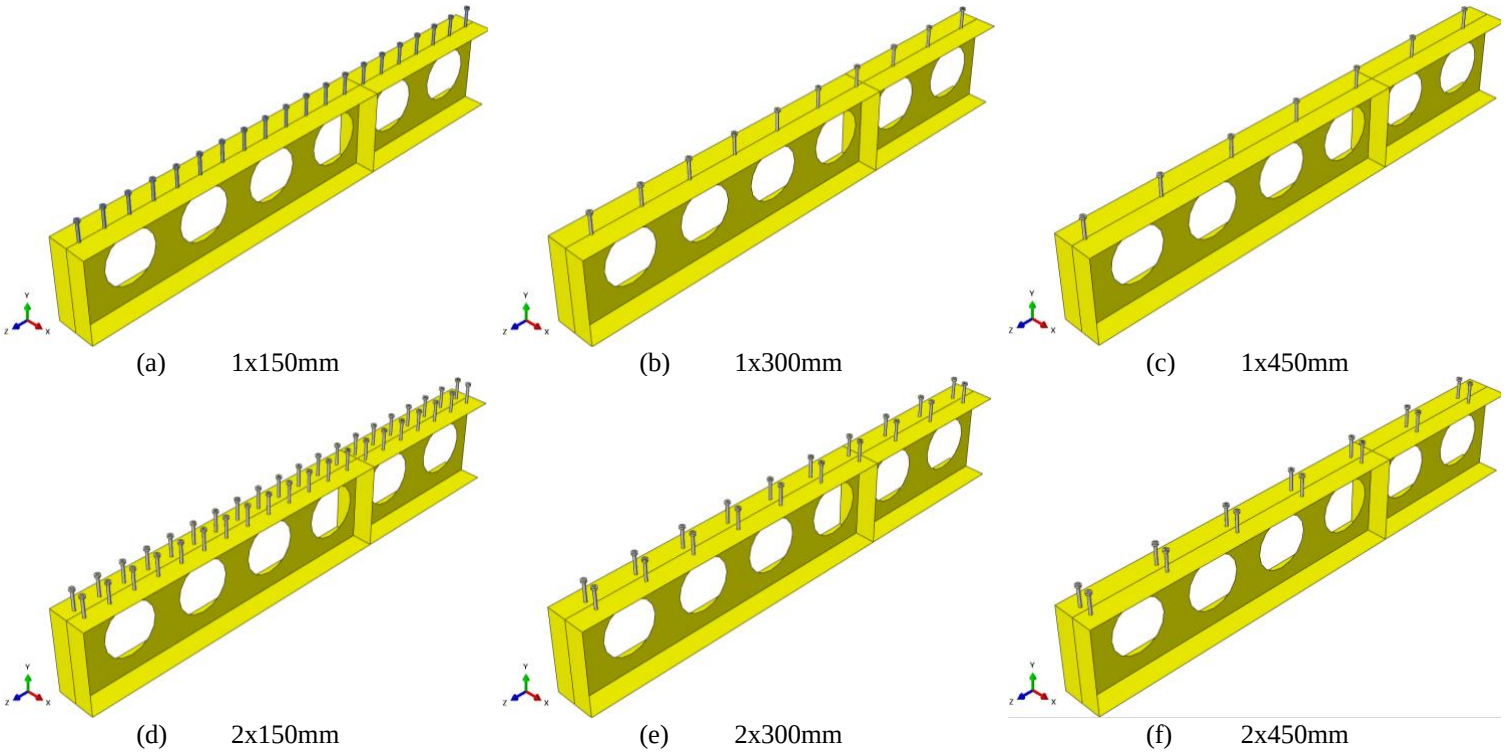

(a) 1x150mm (b) 1x300mm (c) 1x450mm

(d) 2x150mm (e) 2x300mm (f) 2x450mm

Fig. 5: Shear studs spacing for parametric study, considering symmetry at mid-span

9. The infill concrete average strength is 30 MPa, and the PCHCS average strength is 40 MPa; The modulus of elasticity is calculated according to EN 1992-1-1 [63];
10. The length of the composite cellular beam is equal 6m, and the slab width is $L/4$;
11. The composite cellular beams are simply supported and subjected to two-point loads, spaced symmetrically in 2m from supports. Stiffeners were provided at the point of load and support.
12. According to the specifications of EC4 [18] and SCI P355 [15], **Table 2** presents the minimum and maximum values of the interaction degrees (n/n_f) for each series analyzed, in which n is the number of shear studs provided between the points of zero and maximum moment. This value was taken as the number of connectors allocated in the length between the support and the mid-span. The design resistance values of the shear studs were performed according to the constitutive model described in section 4.2. In the case of concrete crushing, the value was reduced by a factor k=0.9. This factor takes account the influence of the confinement of the shear connectors due to the transverse reinforcement, and the geometry of the connectors relative to the hollow core units [38]. The number of shear studs required for full interaction degree (n_f) was taken as the lowest value between the concrete slab compressive resistance and the cellular section tensile resistance.

Table 2 – Interaction degree of models

Model	1x150mm	2x150mm	1x300mm	2x300mm	1x450mm	2x450mm
n	20	40	10	20	7	14
n/n_f	0.40-0.47	0.81-0.93	0.20-0.23	0.40-0.47	0.14-0.16	0.28-0.33
η_{min} [a]	0.41	0.41	0.41	0.41	0.41	0.41

[a]Calculated according to **Eq. (1)**.

4.1. BUCKLING AND POST-BUCKLING ANALYSIS

Buckling and post buckling analyses are widely used in buckling problems [6,61,64–68], such as WPB, that was previously described in the introduction section. The analyses are developed in two stages in ABAQUS® [69], considering the buckling and post-buckling analyses. In the buckling analysis, no material or geometrical imperfections are considered. The deformation mode response in the buckling analysis is used as an initial condition for post buckling analysis, that is, for the application of an initial geometric imperfection. In the post-buckling analysis, the initial geometric imperfection as well as the material and geometric nonlinearity are considered. The initial geometric imperfection is applied with a $d_g/1000$ amplitude, according to the sensitivity analyses carried out by Ferreira et al [6]. The implementation of the initial geometric imperfection is performed using *INITIAL CONDITIONS. Residual stresses are not considered. In the case of composite beams, residual stresses are harmful to study cases in which the composite beams are subjected to a negative bending moment [70,71]. To solve the post-buckling problem, the modified Riks algorithm is used (*Static Riks*). It is necessary to implement the initial arc length, which refers to an initial percentage of the external load. To solve the non-linearity equilibrium equations, the software uses the Newton-Raphson method.

4.2. MATERIALS MODELS

This section presents the constitutive material models used in numerical modeling.

4.2.1 Concrete

The Concrete Damage Plasticity (CDP) [72–74] is used, which is based on the theory of plasticity [75]. The input parameters (**Table 3**) to characterize the plasticity are: dilation angle (ψ), eccentricity (ξ), the ratio of initial equibiaxial compressive yield stress to initial uniaxial compressive yield stress (σ_{b0}/σ_{c0}), the ratio of the second stress invariant on the tensile meridian to that on the compressive meridian (K_c), and the viscosity parameter that represents the relaxation (μ). Carreira and Chu [76,77] stress-strain relationships models are used to represent the behavior of concrete in compression and tension (**Eqs. 3-5**).

Table 3: CDP input parameters

Parameter	Value	References
Ψ (º) (Infill)	40	[30,40,78–81]
Ψ (º) (HCU)	28	[82]
ξ	0.1 (default)	[69,78,79,82]
σ_{b0}/σ_{c0}	1.16 (default)	[69,78,79,82]
K_c	2/3 (default)	[69,78,79,82]
μ (s^{-1})	0.001	[78,79]

$$\frac{\sigma}{f_c}=\frac{\beta_c\left(\varepsilon/\varepsilon_c\right)}{\beta_c-1+\left(\varepsilon/\varepsilon_c\right)^{\beta_c}} \tag{3}$$

$$\frac{\sigma}{f_t}=\frac{\beta_c\left(\varepsilon/\varepsilon_t\right)}{\beta_c-1+\left(\varepsilon/\varepsilon_t\right)^{\beta_c}} \tag{4}$$

$$\beta_c=\left(\frac{f_c}{32.4}\right)^3+1.55\ \ (MPa) \tag{5}$$

4.2.2 Steel

The transverse reinforcement and steel mesh are modeled with elastic-perfectly plastic model (**Fig. 6a**). For the shear studs, the bilinear model (**Fig. 6b**) is used. For cellular beams, the quadrilinear model of Yun and Gardner (**Eqs. 6-10**) [83] is adopted (**Fig. 6c**). The implementation of the stress- strain relationship must be done with the real values, according to the **Eqs. (11-12).**

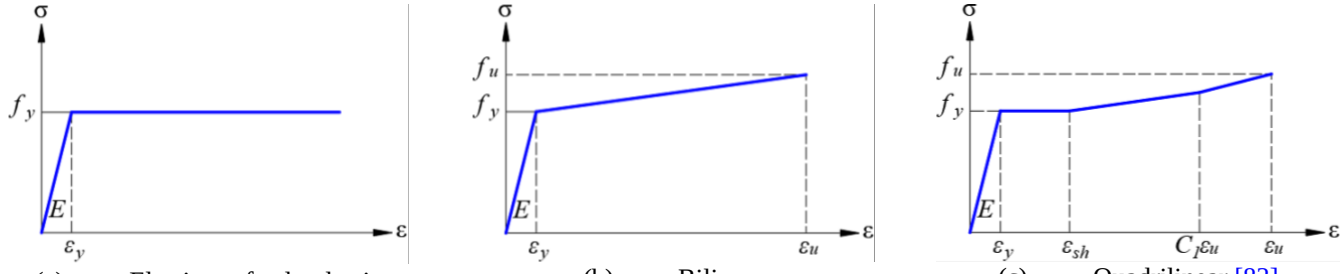

(a) Elastic-perfectly plastic (b) Bilinear (c) Quadrilinear [83]

Fig. 6: Stress-strain relationship for steel [30]

$$f(\varepsilon)=\begin{cases} E\varepsilon, \varepsilon \le \varepsilon_y \\ f_y, \varepsilon_y < \varepsilon \le \varepsilon_{sh} \\ f_y + E_{sh}(\varepsilon - \varepsilon_{sh}), \varepsilon_{sh} < \varepsilon \le C_1\varepsilon_u \\ f_{C_1\varepsilon_u} + \left(\dfrac{f_u + f_{C_1\varepsilon_u}}{\varepsilon_u - C_1\varepsilon_u}\right), C_1\varepsilon_u < \varepsilon \le \varepsilon_u \end{cases} \quad (6)$$

$$\varepsilon_u = 0.6\left(1-\frac{f_y}{f_u}\right), \varepsilon_u \ge 0.06 \quad (7)$$

$$\varepsilon_{sh} = 0.1\frac{f_y}{f_u} - 0.055, 0.015 < \varepsilon_{sh} \le 0.03 \quad (8)$$

$$C_1 = \frac{\varepsilon_{sh} + 0.25(\varepsilon_u - \varepsilon_{sh})}{\varepsilon_u} \quad (9)$$

$$E_{sh} = \frac{f_u - f_y}{0.4(\varepsilon_u - \varepsilon_{sh})} \quad (10)$$

$$\sigma^{true} = \sigma^{nom}\left(1+\varepsilon^{nom}\right) \quad (11)$$

$$\varepsilon^{true} = \ln\left(1+\varepsilon^{nom}\right) \quad (12)$$

4.3. INTERACTION

The modeling of hollow core slabs is complex. As an example, it can be cited the studies carried out by the references [82,84,85]. In Nguyen et al. [82] a three-dimensional numerical model of hollow core slabs was developed to investigate web-shear behavior. The steel strands were discretized with truss elements with a linear stress distribution. The authors consider the perfect bond between the steel strands and the precast concrete. The results of the numerical models presented an error of a maximum of 15% in comparison with the results of the experimental models. Subsequently, Nguyen and Tan [85] used the same modeling technique, however, considering hollow core slabs subjected to fire. This same technique was shown to be coherent when compared with the experimental results. In Elharouney et al. [84] the numerical model of hollow core slabs was developed in two steps. The first step consisted of applying the prestressing forces to the strands. In the second step, the boundary conditions were applied, as well as the external loading by displacement control.

The previous studies aimed to investigate the ultimate resistance of hollow core slabs. In the present work, PCHCS and PCHCSCT are disposed transversely in relation to the cellular profile, considering for this only an effective width. In this context, the effect of prestressing forces can be neglected. This modeling technique was previously used by references [30,31,36,62], which proved to be adequate for the representation of physical models in numerical models. Thus, three types of interaction between the contact surfaces are used. The tie constraint, which allows to simulate the perfect bond between the contact surfaces, it is applied to the surface between on the bottom surfaces of the shear studs and the upper flange, and between the precast and in-situ infill concrete [40]. The *Embedded region* is used to specify that an element is embedded in another element. This type of interaction is applied between the concrete and the transverse reinforcement, as well as the concrete and steel mesh. *Normal/tangential behavior* allows

displacement in the normal and tangential direction to the contact surface plane. It is applied between the gap- shear studs, and the slab-cellular beam surfaces. This technique has already been used by references [86,87]. The tangential behavior is based on the Coulomb friction model. The friction coefficients are taken equal to 0.2 and 0.3, for gap-shear studs, and slab-cellular beam interfaces, respectively [6,40,61,80,88].

4.4. BOUNDARY CONDITIONS AND DISCRETIZATION

The boundary conditions are applied according to references [6,40,61,62], considering symmetry at mid-span. For this, the vertical displacement (Uy=0) in the support, the lateral displacement (Ux=0) at the ends of the slab, and the mid-span (Uz=URx=URy=0) are restrained. Regarding the discretization, the dimensions of elements are taken according to others studies [6,61,80,82,89,90]. The cellular beams are discretized with S4R element, which is a quadrilateral element with four nodes and reduced integration. The shear studs, the PCHCS and the in-situ elements, were discretized by the solid element C3D8R, which has eight nodes and reduced integration. The transverse reinforcement as well as steel mesh are discretized with truss elements (T3D2), with two nodes and linear displacement. **Fig. 7a** shows the boundary conditions and discretization of composite cellular beams with PCHCS or PCHCS. **Fig. 7b** illustrates the discretization of the shear studs and gap.

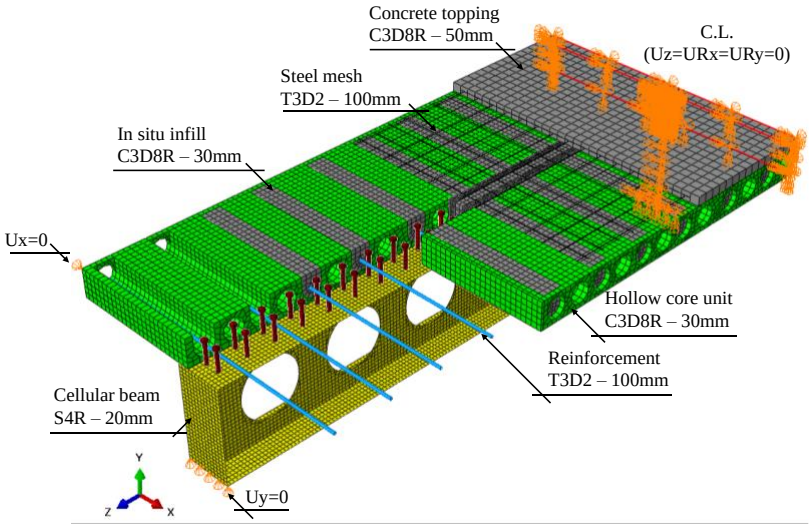

(a) Composite cellular beam with PCHCS(CT)

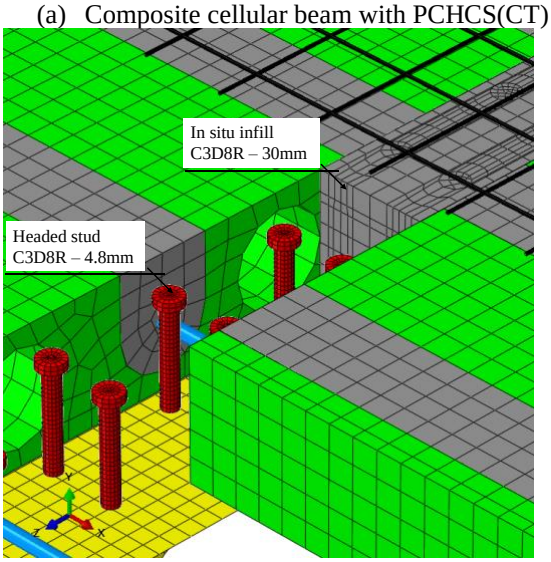

(b) Shear studs and gaps illustration

Fig. 7: Boundary conditions and discretization

5. RESULTS AND DISCUSSION

In total, 240 numerical models were developed for this parametric study. Some examples of the failure modes are illustrated in **Fig. 8.** Although the predominant failure mode observed was web post buckling combined with the plastic mechanism (WPB+PM) (**Fig. 8a)** and the formation of the Vierendeel mechanism (VM) (**Fig. 8b)**, these failure modes have been observed in combination with the shear stud rupture (WPB+PM* and VM*) (**Fig. 8c)**. The results are discussed, considering 150mm, 300mm and 450mm of spacing. At the end of the results and discussion section, a general analysis is made with the presentation of the results.

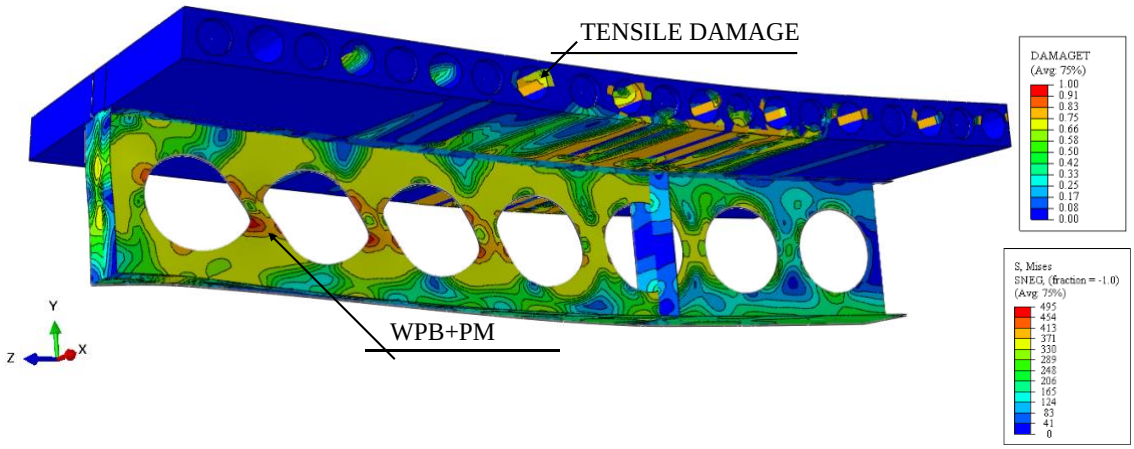

(a) WPB+PM: D_o/d=0.9 and p/D_o=1.3 with PCHCS and 2x150mm of spacing

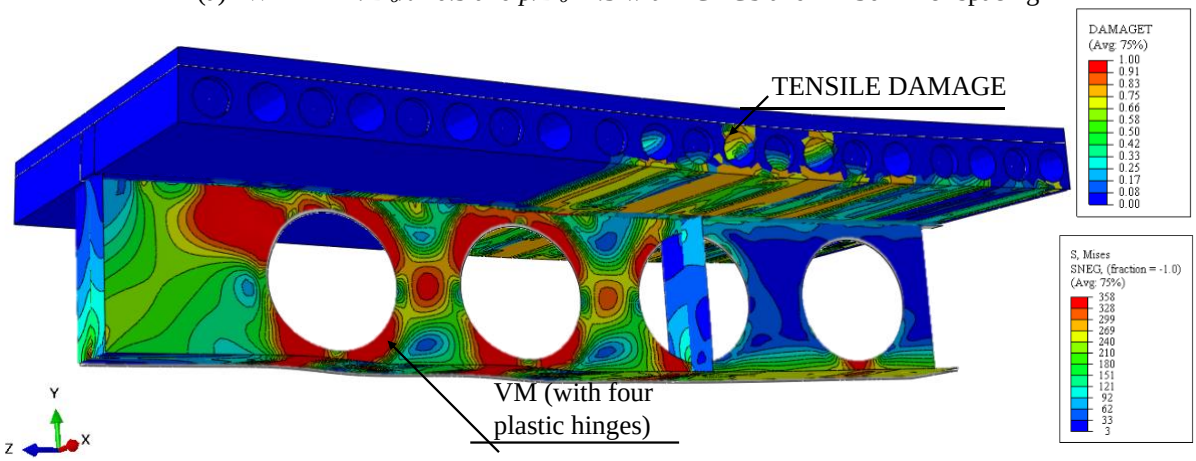

(b) VM: D_o/d=1.5 and p/D_o=1.5 with PCHCSCT and 1x300mm of spacing

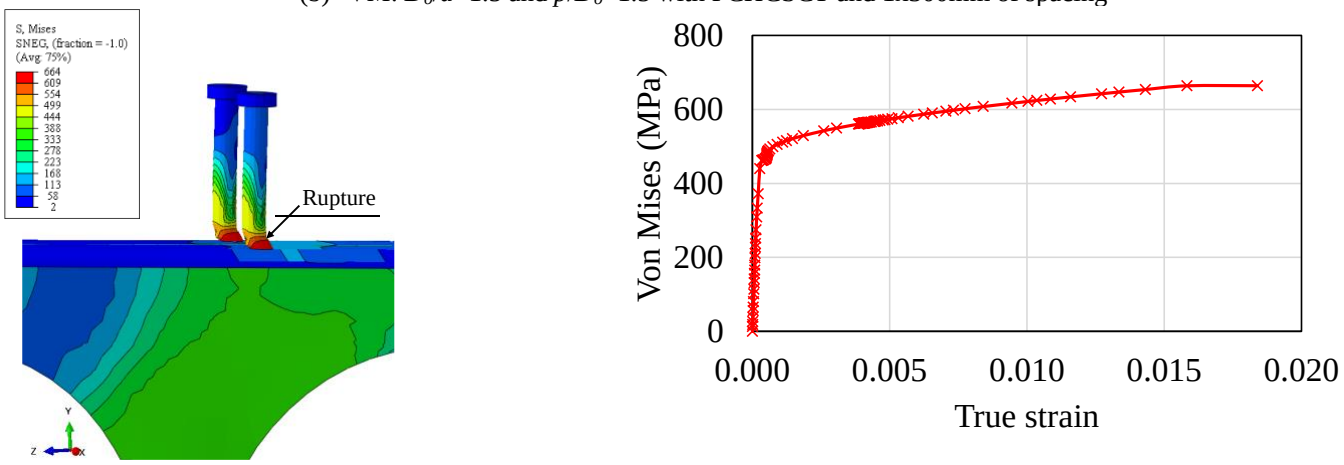

(c) Shear stud rupture

Fig. 8: Failure modes

5.1. 150MM OF SPACING

The total number of shear studs (n), from the support to the mid-span, is 20 and 40 for 1x150mm and 2x150mm, respectively. For the D_o/d=0.8-1.0, D_o/d=1.1; p/D_o=1.2-1.3 and D_o/d=1.2; p/D_o=1.4-1.5 models, the total number of shear studs above the opening (n_h) is 2 and 4 for 1x150mm and 2x150mm, respectively. For the D_o/d=1.1; p/D_o=1.4-1.5 and D_o/d=1.2; p/D_o=1.2-1.3 models, n_h is 3 and 6 for 1x150mm and 2x150mm, respectively. Notably, the larger the opening diameter, the greater n_h.

Regarding the development of the analyses, for the mid-span vertical displacement at 15.2±0.3mm (1x150mm) and 15.0±0.3mm (2x150mm), both the tees and the shear studs had already reached the yield strength. The global shear force values were 291.7±46.9kN and 304.5±51.1kN, for 1x150mm and 2x150mm, respectively. For the tees, the von Mises stresses were 347.7±1.1MPa and 347.7±1.2MPa, for 1x150mm and 2x150mm, respectively. Considering the shear studs, these stresses were 480.8±4.6MPa and 470.1±10.4MPa, for 1x150mm and 2x150mm, respectively. On the PCHCS, the upper regions close to the support, the lower part close to the loading application point, and the cores without filled were already damaged. The relative slip between the PCHCS and the cellular beam was 0.2±0.1mm and null, for 1x150mm and 2x150mm, respectively. With increasing loading, for the mid-span vertical displacement at 30.3±0.8mm (1x150mm), the measured values of the global shear force were 393.2±76.8kN (1x150mm) and 428.9±82.8kN (2x150mm). Notably, there was an increase in von Mises stresses. For the tees, the von Mises stresses were 379.4±22.2MPa (1x150mm) and 383.9±23.0MPa (2x150mm), and for the shear studs were 547.7±29.7MPa (1x150mm) and 485.2±5.3MPa (2x150mm). Regarding the PCHCS, there was an increase in the damaged region, and the relative slip between the PCHCS and the cellular beam was 0.9±0.3mm and 0.1±0.1mm, for 1x150mm and 2x150mm, respectively. Finally, in the ultimate resistance, the mid-span vertical displacements measured were 40.2±7.4mm (1x150mm) and 38.9±9.5mm (2x150mm). In these models, the stopping criterion adopted was verified when the peak load was reached. Thereafter, as the displacement increases, the load decreases. The global shear force was 419.3±85.7kN and 454.1±92kN, for 1x150mm and 2x150mm, respectively. For the tees, the von Mises stresses were 419.1±27.3MPa (1x150mm) and 417.2±30.8MPa (2x150mm). For the shear studs, the von Mises stresses were 590.0±30.5MPa (1x150mm) and 496.8±17.8MPa (2x150mm). It was observed in this circumstance, for 2x150mm, the stresses were lower than in relation to 1x150mm models. This can be explained as the shear studs have the capacity to absorb the shear flow at the steel-concrete interface. In this context, the relative slip between the PCHCS and the cellular beam was 1.4±0.4mm and 0.1±0.1mm, for 1x150mm and 2x150mm, respectively. An increase in damage was observed in the upper part of the slab on the ultimate resistance (**Fig. 9)**, especially in models where the end post width (b_{we}) was greater than the width of the others web posts (b_w).

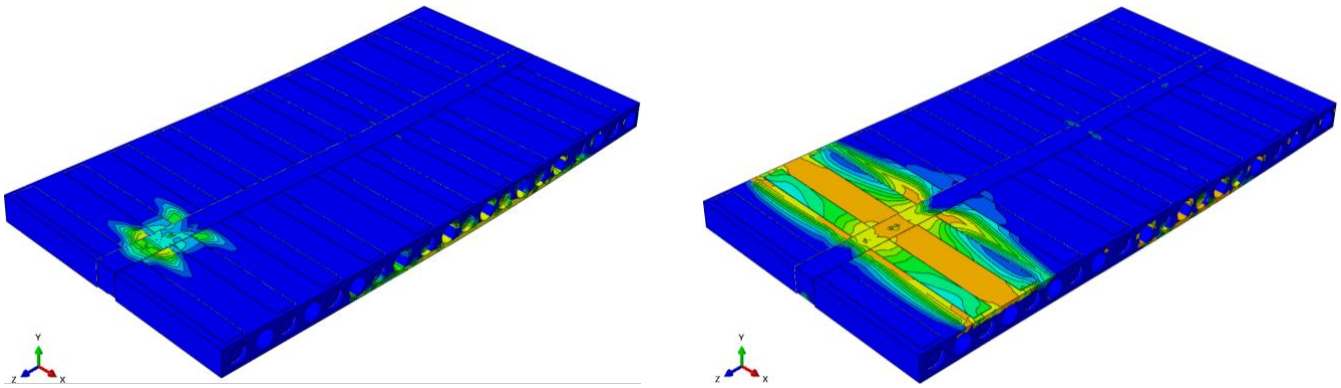

(a) D_o/d=0.8; p/D_o=1.3 and b_{we}/b_w=1.5 (b) D_o/d=0.8; p/D_o=1.5 and b_{we}/b_w=3.9

Fig. 9: Tensile damage above the supports, considering PCHCS models

Concerning the composite cellular beams with PCHCSCT, there was an increase in the axial resistance of the PCHCS due to the presence of the CT. In this context, the relative difference between the axial resistance of the PCHCSCT and the connection (nP_{sc}) increased. Regarding the analyses, the behavior was similar to composite cellular beams with PCHCS models. For the mid-span vertical displacement at 15.3±0.4mm (1x150mm) and 15.1±0.4mm (2x150mm), the global shear force, the von Mises stresses of tees and shear studs, and the relative slips were 352.3±51.8kN; 347.9±1.2MPa; 496.8±10.9MPa; 0.6±0.2mm and 389.3±65.3kN; 348.1±1.0MPa; 481.0±5.9MPa; 0.1±0.1mm, for 1x150mm and 2x150mm models, respectively. With the mid-span vertical displacements at 30.3±0.7mm (1x150mm) and 30.2±0.5mm (2x150mm), the global shear force, the von Mises stresses of tees and shear studs, and the relative slips were 446.1±86.0kN; 390.1±23.1MPa; 601.4±15.9MPa; 1.7±0.3mm and 485.5±102.4kN; 409.3±22.9MPa; 494.2±11.7MPa; 0.3±0.2mm, for 1x150mm and 2x150mm models, respectively. In the ultimate resistance, for the mid-span vertical displacements at 43.2±9.2mm (1x150mm) and 32.8±4.5mm (2x150mm), the global shear force, the von Mises stresses of tees and shear studs, and the relative slips were 474.8±77.2kN; 439.6±39.9MPa; 644.0±24.8MPa; 2.6±0.4mm and 508.2±90.9kN; 421.5±33.8MPa; 502.4±13.6MPa; 0.4±0.3mm, for 1x150mm and 2x150mm models, respectively.

Fig. 10 shows the influence of the concrete topping, considering the global shear force differences between the PCHCSCT and PCHCS models ($V_{PCHCSCT}$-V_{PCHCS}). According to the illustrations (**Fig. 10a-e**), for the models analyzed, the models with concrete topping obtained greater resistance in the structural system ($V_{PCHCSCT}$-V_{PCHCS} >0). Such observation was previously reported by Ferreira et al. [30]. The variations in the differences tend to be smaller when the failure modes were defined by the WPB+PM. In the other models, the variations of the differences tend to increase, mainly for the analyses in which the VM was observed. The maximum difference with a value equal to 113kN was observed for the model D_o/d=1.0 and p/D_o=1.2 with 1x150mm, which was observed WPB+PM. The minimum difference was analyzed for the D_o/d=0.8 and p/D_o=1.3 models with 2x150mm, which obtained VM for PCHCSCT model, and WPB+PM for PCHCS model. Such analyses demonstrate that the concrete topping influenced the change in the failure mode of the composite cellular beams.

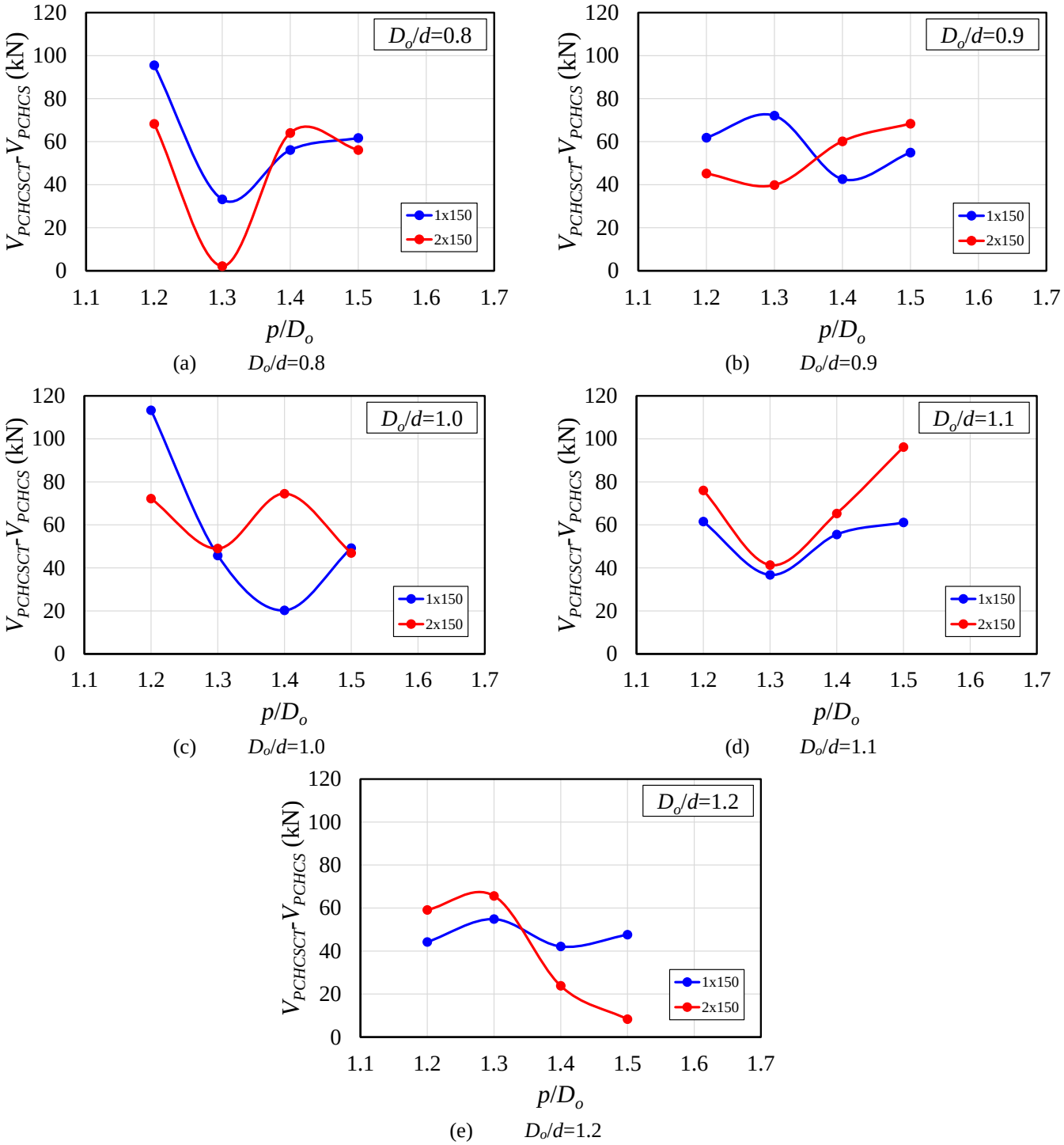

Fig. 10: The influence of concrete topping for models with 150mm of shear studs spacing

Fig. 11 illustrates the shear resistance of the models analyzed as a function of key parameters, such as the D_o/d and p/D_o. As shown in the illustration, for most of the cases, the 2x150mm models presented greater or equal shear resistance compared to 1x150mm models. This shows that the WPB resistance is also influenced by the composite action, that is directly relevant to the number of connectors above the opening. In addition, as shown in the illustration, a drop in resistance is observed for the models D_o/d=1.0 and p/D_o=1.2 (**Fig. 11c**), and D_o/d=1.2 and p/D_o=1.2(**Fig. 11e**) in compared to the models p/D_o=1.4. This was due to the fact that the end-post width of the models p/D_o=1.4 are longer than the end-post width of the models p/D_o=1.5. This was reported in Ferreira et al. [6]. The failure modes analyzed are presented (**Table 4**).

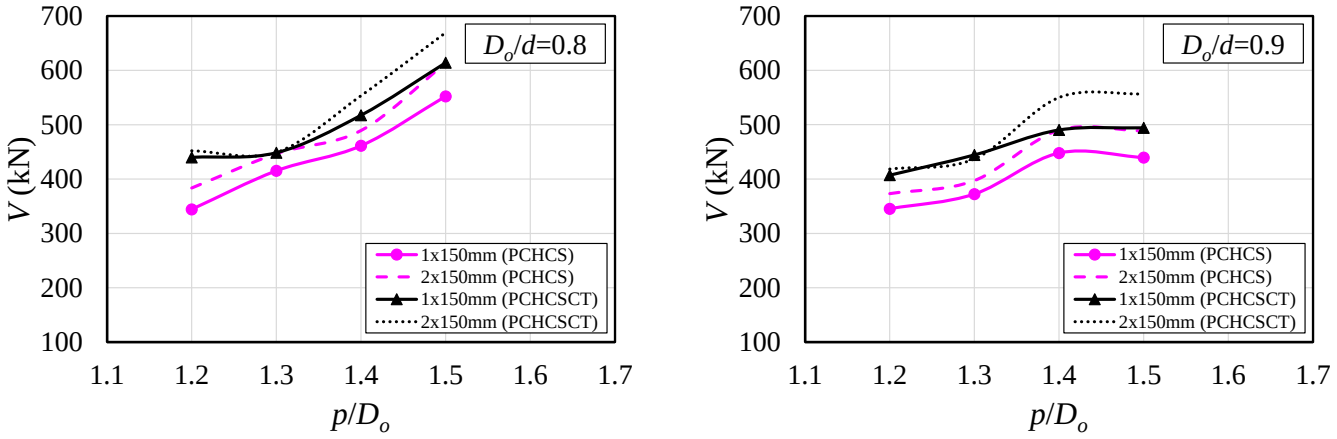

(a) D_o/d=0.8

(b) D_o/d=0.9

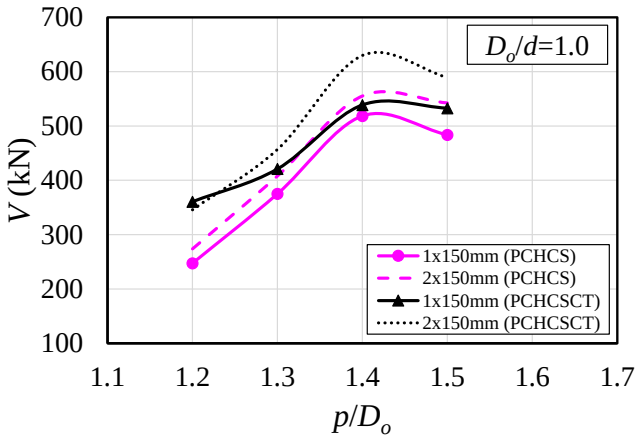

(c) D_o/d=1.0

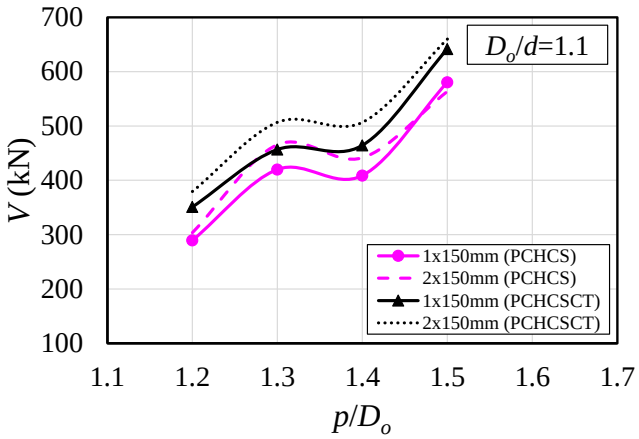

(d) D_o/d=1.1

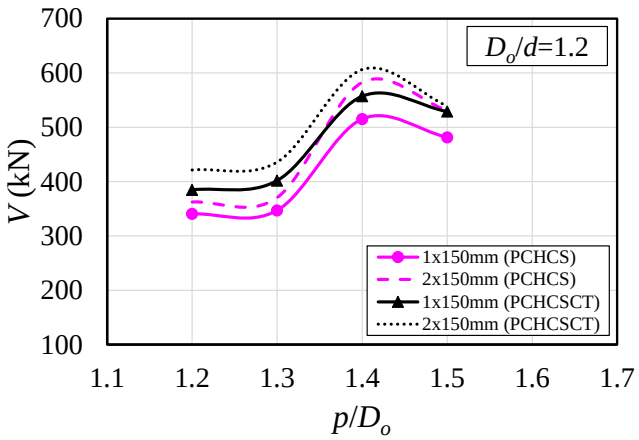

(e) D_o/d=1.2

Fig. 11: Results for models with 150mm of shear studs spacing, considering PCHCS and PCHCSCT

Table 4 – Failure modes for 1x150mm and 2x150mm models

D_o/d	p/D_o	1x150mm		2x150mm	
		PCHCSCT	PCHCS	PCHCSCT	PCHCS
0.8	1.2	WPB+PM*	VM	WPB+PM	VM
	1.3	WPB+PM*	WPB+PM	VM	WPB+PM
	1.4	WPB+PM	WPB+PM	WPB+PM	WPB+PM
	1.5	WPB+PM*	WPB+PM	WPB+PM	WPB+PM
0.9	1.2	WPB+PM*	WPB+PM	WPB+PM	WPB+PM
	1.3	WPB+PM*	WPB+PM	WPB+PM	WPB+PM
	1.4	WPB+PM	WPB+PM	WPB+PM	WPB+PM
	1.5	WPB+PM	WPB+PM	WPB+PM	WPB+PM
1.0	1.2	WPB+PM*	WPB+PM	WPB+PM	WPB+PM
	1.3	WPB+PM*	WPB+PM	WPB+PM	WPB+PM
	1.4	WPB+PM	WPB+PM	VM	WPB+PM
	1.5	WPB+PM	WPB+PM	VM	WPB+PM
1.1	1.2	WPB+PM*	WPB+PM	WPB+PM	WPB+PM
	1.3	WPB+PM	WPB+PM	WPB+PM	WPB+PM
	1.4	VM	WPB+PM	WPB+PM	WPB+PM
	1.5	VM*	WPB+PM	VM	VM
1.2	1.2	WPB+PM*	VM	WPB+PM	VM
	1.3	VM	VM	VM	VM
	1.4	VM*	VM	VM	VM
	1.5	VM*	VM	VM	VM

*The shear stud rupture occurred.

5.2. 300MM OF SPACING

In these analyses, n is 10 and 20 for 1x300mm and 2x300mm, respectively. For the D_o/d=0.8;1.0-1.1 and p/D_o=1.2-1.5, D_o/d=0.9 and p/D_o=1.2;1.4-1.5, D_o/d=1.2 and p/D_o=1.2-1.3;1.5 models, n_h is 1 and 2 for 1x300mm and 2x300mm, respectively. For the D_o/d=0.9; p/D_o=1.3 and D_o/d=1.2; p/D_o=1,4, n_h is 2 and 4 for 1x300mm and 2x300mm, respectively.

The structural behaviors of the composite cellular beams with PCHCS, considering 1x300mm and 2x300mm, were similar to the previous models described in section 5.1. For the mid-span vertical displacement at 15.3±0.4mm (1x300mm) and 15.2±0.3mm (2x300mm), the global shear force, the von Mises stresses of tees and shear studs, and the relative slips were 258.1±39.2kN; 347.3±1.2MPa; 520.6±22.2MPa; 0.9±0.2mm and 289.6±48.6kN; 347.8±1.3MPa; 479.7±4.2MPa; 0.3±0.1mm for 1x300mm and 2x300mm models, respectively. With the mid-span vertical displacements at 30.1±0.5mm (1x300mm) and 30.2±0.3mm (2x300mm), the global shear force, the von Mises stresses of tees and shear studs, and the relative slips were 342.7±71.3kN; 370.1±18.7MPa; 598.2±22.5MPa; 2.1±0.4mm and 397.3±74.1kN; 377.9±21.6MPa; 533.7±21.3MPa; 0.9±0.3mm for 1x300mm and 2x300mm models, respectively. In the ultimate resistance, for the mid-span vertical displacements at 39.0±5.3mm (1x300mm) and 40.5±8.4mm (2x300mm), the global shear force, the von Mises stresses of tees and shear studs, and the relative slips were 365.0±77.8kN; 411.9±27.7MPa; 640.5±23.6MPa; 2.7±0.6mm and 414.9±84.7kN; 420.2±32.9MPa; 571.9±36.9MPa; 1.4±0.5mm for 1x300mm and 2x300mm models, respectively. An important observation in the ultimate resistance was in relation to the decrease

in global shear resistance that the present discussion obtained in relation to the previous one (**Table 5**). **Fig. 12** shows an example, considering the D_o/d=0.9 and p/D_o=1.5 model.

Table 5 – Global shear force comparative analyses between the present and previous models, considering PCHCS (in kN)

$V_{(1x150)}$	$V_{(1x300)}$	$V_{(1x300)}/V_{(1x150)}$	$V_{(2x150)}$	$V_{(2x300)}$	$V_{(2x300)}/V_{(2x150)}$
419.3±85.7	365.0±77.8	0.87	454.1±92kN	414.9±84.7	0.91

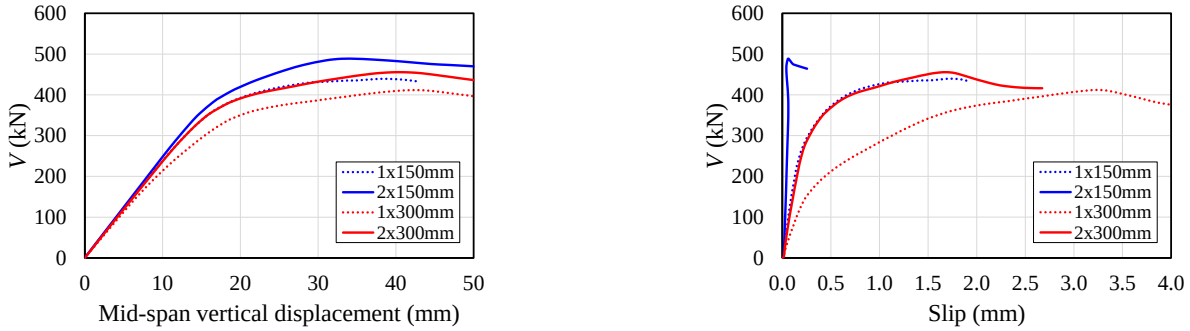

(a) Global shear force vs. mid-span vertical displacement (b) Global shear force vs. slip

Fig. 12: D_o/d=0.9 and p/D_o=1.5 models with PCHCS. Failure mode: WPB+PM

In view of the analyses carried out on the composite cellular beams with PCHCSCT, considering 1x300mm and 2x300mm, the structural behaviors were similar to described in section 5.1. For the mid-span vertical displacement at 15.3±0.4mm (1x300mm) and 15.5±0.3mm (2x300mm), the global shear force, the von Mises stresses of tees and shear studs, and the relative slips were 290.1±42.2kN; 347.3±1.2MPa; 554.0±22.6MPa; 1.4±0.2mm and 348.6±50.7kN; 348.1±1.6MPa; 494.9±11.8MPa; 0.6±0.2mm for 1x300mm and 2x300mm models, respectively. With the mid-span vertical displacements at 30.2±0.7mm (1x300mm and 2x300mm), the global shear force, the von Mises stresses of tees and shear studs, and the relative slips were 349.4±59.2kN; 376.9±20.0MPa; 636.7±26.2MPa; 2.8±0.3mm and 436.5±82.2kN; 395.5±21.6MPa; 581.5±25.1MPa; 1.7±0.4mm for 1x300mm and 2x300mm models, respectively. In the ultimate resistance, for the mid-span vertical displacements at 34.1±4.8mm (1x300mm) and 46.8±11.2mm (2x300mm), the global shear force, the von Mises stresses of tees and shear studs, and the relative slips were 395.9±62.0kN; 387.5±32.7MPa; 663.6±1.7MPa; 3.3±0.1mm and 483.7±70.7kN; 444.6±44.3MPa; 641.5±25.5MPa; 2.7±0.5mm for 1x300mm and 2x300mm models, respectively. **Table 6** and **Fig. 13** shows an example of comparations of the ultimate global shear force between the present and previous analyses.

Table 6 – Global shear force comparative analyses between the present and previous models with PCHCSCT (in kN)

$V_{(1x150)}$	$V_{(1x300)}$	$V_{(1x300)}/V_{(1x150)}$	$V_{(2x150)}$	$V_{(2x300)}$	$V_{(2x300)}/V_{(2x150)}$
474.8±77.2	395.9±62.0	0.83	508.2±90.9	483.7±70.7	0.95

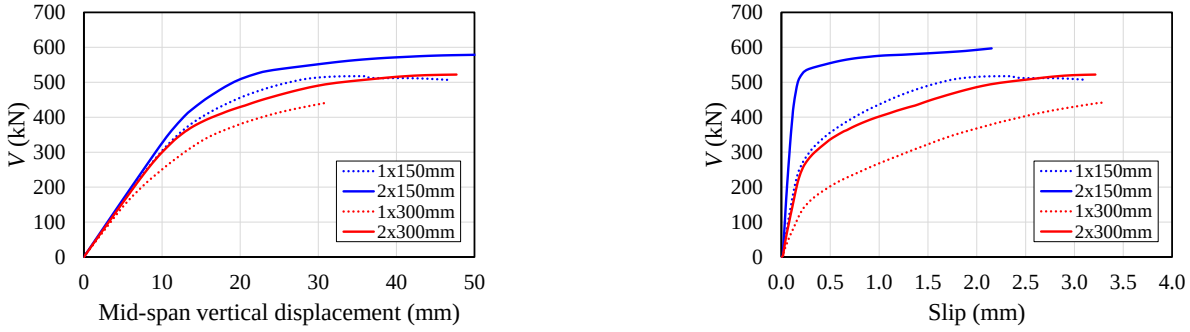

(a) Global shear force vs. mid-span vertical displacement (b) Global shear force vs. slip

Fig. 13: D_o/d=0.8 and p/D_o=1.4 models with PCHCSCT. Failure modes: WPB+PM (150mm) and WPB+PM* (300mm)

Fig. 14 illustrates the influence of the concrete topping ($V_{PCHCSCT}$-V_{PCHCS}). As shown in the figures (**Fig. 14a, Fig. 14c and Fig. 14d**), in some models the difference between the PCHCSCT and PCHCS models was negative ($V_{PCHCSCT}$-V_{PCHCS}<0). This was verified specifically for models p/D_o=1.5; D_o/d=0.8; 1.0 and 1.1 with 1x300mm, in which their failures modes were: VM (p/D_o=1.5; D_o/d=0.8;) and VM* (p/D_o=1.5; D_o/d=1.0-1.1) for PCHCSCT models, and WPB+PM* (p/D_o=1.5; D_o/d=0.8;1.1) and WPB+PM (p/D_o=1.5; D_o/d=1.0) for PCHCS models. It has been observed so far that, although the concrete topping has increased the resistance in previous analyses (**Fig. 10**), in the present models, the presence of the concrete topping and the reduced number of shear studs, contributed to the failure mode occurring in the connection, a factor that reduced the resistance of the global shear force. The maximum difference with a value equal to 126kN was observed for the model D_o/d=1.0 and p/D_o=1.2 with 2x300mm, which was verified WPB+PM for PCHCS model and WPB+PM* for PCHCSCT model. The minimum difference, which was of 22kN, occurred for the D_o/d=1.1 and p/D_o=1.5 model with 1x300mm. In these models, the failure modes analyzed were VM, and WPB+PM* for PCHCSCT and PCHCS models, respectively.

Fig. 15 illustrates the shear resistance of the models analyzed as a function of key parameters, such as the D_o/d and p/D_o. As shown in the illustration, it is observed that the models with 2x300mm presented greater resistance to global shear force than the models with 1x300mm. Also, similarly to what was presented and discussed in **Fig. 11c** and **Fig. 11e**, there was a drop in resistance as a function of the end-post width (**Fig 15c** and **Fig. 15e**). The failure modes analyzed are presented (**Table 7**).

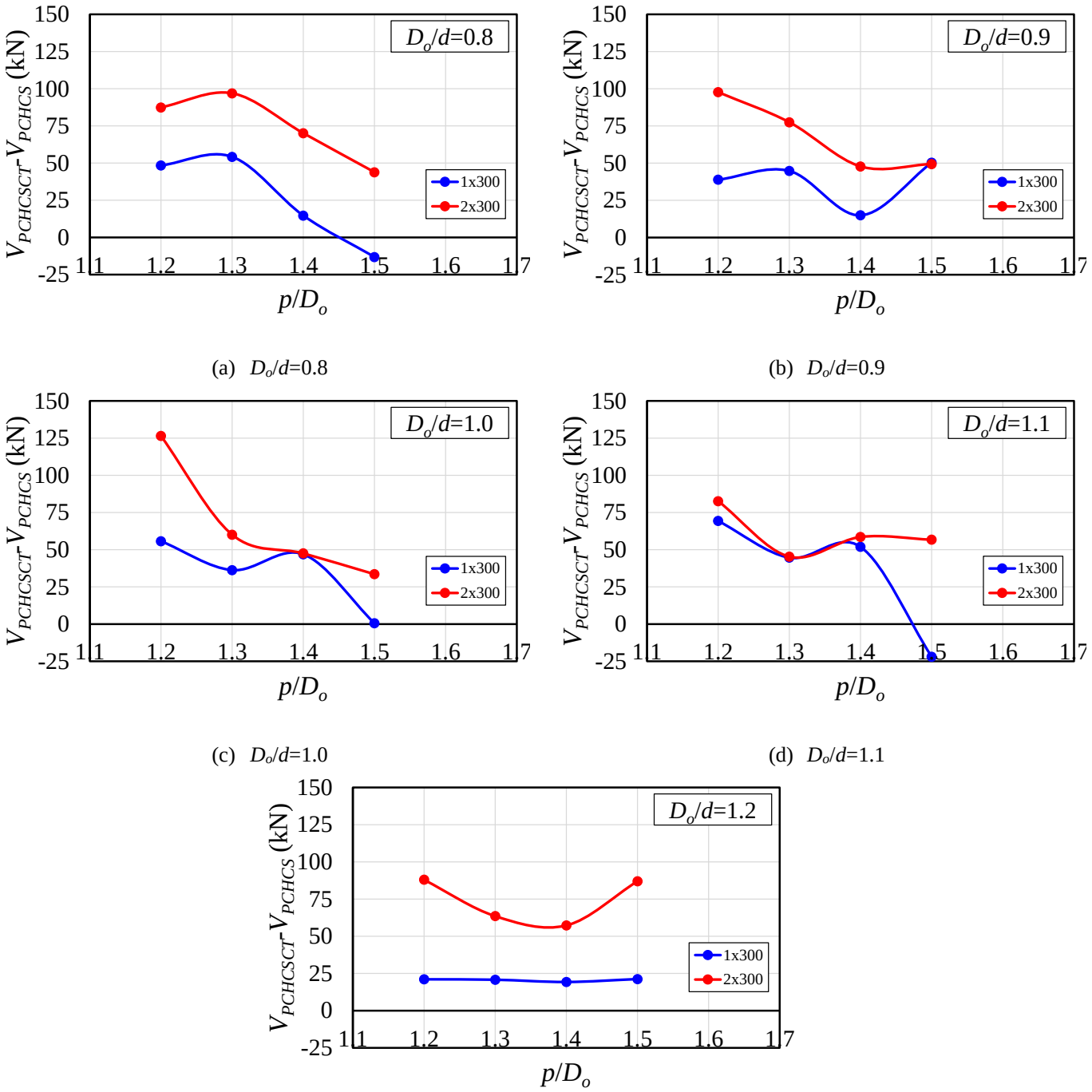

(a) D_o/d=0.8

(b) D_o/d=0.9

(c) D_o/d=1.0

(d) D_o/d=1.1

(e) D_o/d=1.2

Fig. 14: The influence of concrete topping for models with 300mm of shear studs spacing

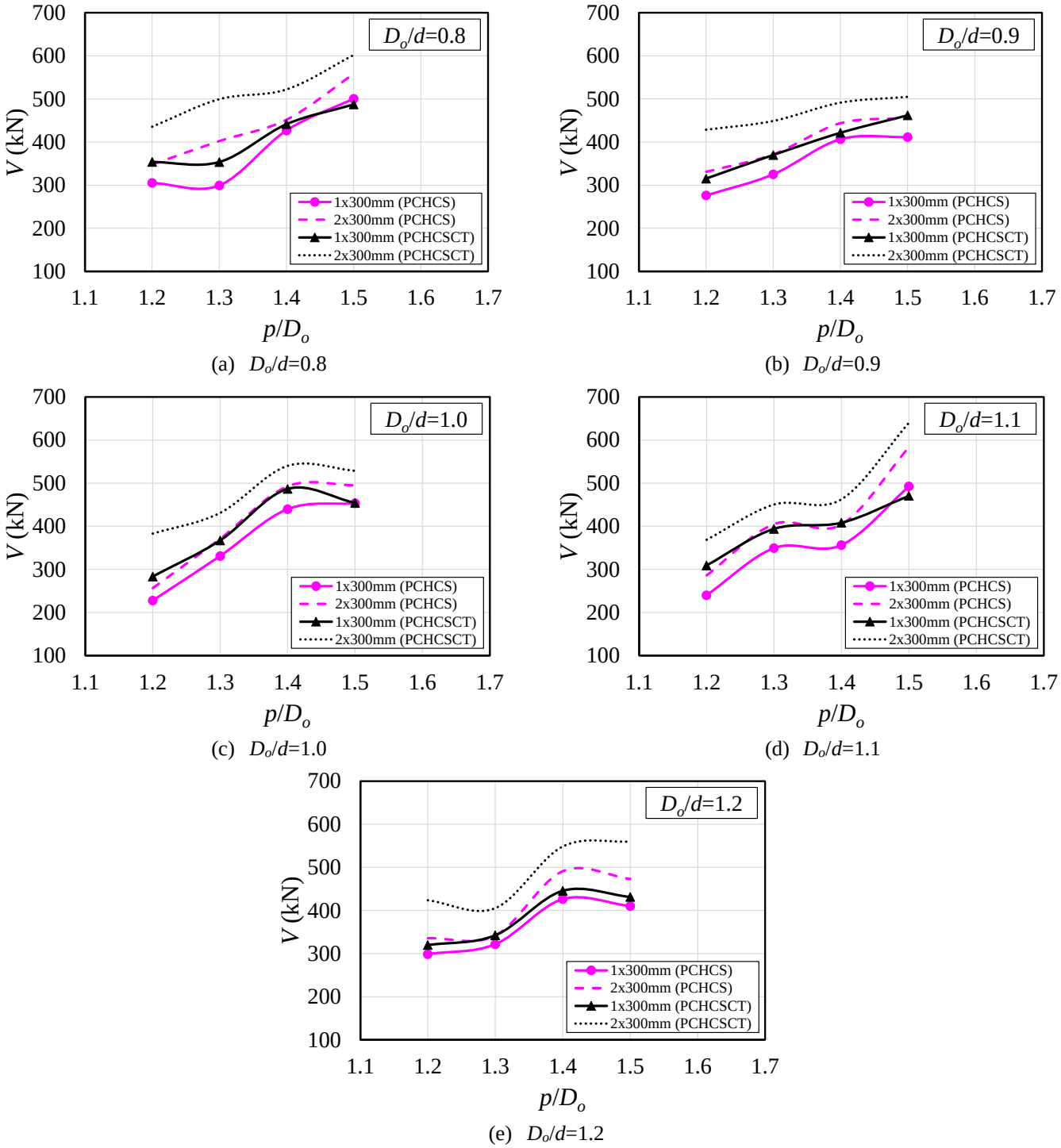

(a) D_o/d=0.8 (b) D_o/d=0.9

(c) D_o/d=1.0 (d) D_o/d=1.1

(e) D_o/d=1.2

Fig. 15: Results for models with 300mm of shear studs spacing, considering PCHCS and PCHCSCT

Table 7 – Failure modes for 1x300mm and 2x300mm models

D_o/d	p/D_o	1x300mm		2x300mm	
		PCHCSCT	PCHCS	PCHCSCT	PCHCS
0.8	1.2	VM*	VM	WPB+PM*	VM
	1.3	VM*	VM*	WPB+PM*	WPB+PM
	1.4	WPB+PM*	WPB+PM	WPB+PM*	WPB+PM
	1.5	VM	WPB+PM*	WPB+PM	WPB+PM
0.9	1.2	VM*	VM	WPB+PM*	VM
	1.3	WPB+PM*	WPB+PM	WPB+PM*	WPB+PM
	1.4	VM*	WPB+PM	WPB+PM	WPB+PM
	1.5	VM*	WPB+PM	WPB+PM	WPB+PM
1.0	1.2	WPB+PM*	WPB+PM	WPB+PM*	WPB+PM
	1.3	WPB+PM*	WPB+PM	WPB+PM	WPB+PM
	1.4	VM*	WPB+PM	VM	WPB+PM
	1.5	VM*	WPB+PM	VM	WPB+PM
1.1	1.2	VM*	WPB+PM	WPB+PM*	WPB+PM
	1.3	VM*	WPB+PM	WPB+PM	WPB+PM
	1.4	VM*	WPB+PM	VM	WPB+PM
	1.5	VM*	WPB+PM*	VM*	WPB+PM
1.2	1.2	VM*	VM	WPB+PM*	WPB+PM
	1.3	VM*	VM	VM	VM
	1.4	VM*	VM*	VM	VM
	1.5	VM*	VM*	VM*	VM

*The shear stud rupture occurred.

5.3. 450MM OF SPACING

In these analyses, n is 7 and 14, for 1x450mm and 2x450mm, respectively. For the D_o/d=0.8 and p/D_o=1.3 and 1.5; D_o/d=0.9 and p/D_o=1.3 and 1.5; D_o/d=1.0 and p/D_o=1.2 and 1.4; D_o/d=1.1 and p/D_o=1.3; D_o/d=1.2 and p/D_o=1.5, there are no shear studs above the opening closest to the support (n_h=0). For the other models, n_h is 1 and 2, considering 1x450mm and 2x450mm, respectively.

Regarding the analyses, for the mid-span vertical displacement at 15.5±0.4mm (1x450mm) and 15.3±0.5mm (2x450mm), the global shear force, the von Mises stresses of tees and shear studs, and the relative slips were 244.1±35.7kN; 347.2±1.1MPa; 533.0±16.4MPa; 1.1±0.2mm and 275.0±43.2kN; 347.5±1.1MPa; 484.5±6.9MPa; 0.5±0.2mm for 1x450mm and 2x450mm models, respectively. For mid-span vertical displacements at 30.3±0.8mm (1x450mm) and 30.3±0.5mm (2x450mm), the global shear force, the von Mises stresses of tees and shear studs, and the relative slips were 337.8±61.5kN; 365.7±15.2MPa; 611.1±21.0MPa; 2.4±0.4mm and 366.9±72.0kN; 372.6±19.7MPa; 558.1±25.0MPa; 1.4±0.3mm for 1x450mm and 2x450mm models, respectively. In the ultimate resistance, with the mid-span vertical displacements at 40.7±5.5mm (1x450mm) and 39.8±4.6mm (2x450mm), the global shear force, the von Mises stresses of tees and shear studs, and the relative slips were 358.2±71.0kN; 412.1±34.3MPa; 660.4±8.0MPa; 3.2±0.5mm and 398.1±82.7kN; 415.0±24.5MPa; 614.6±43.1MPa; 1.9±0.5mm for 1x450mm and 2x450mm models, respectively. **Table 8** and **Fig. 16** shows an example of comparations of the ultimate global shear force between the present (1x450mm and 2x450mm) and previous analyses (1x300mm and 2x300mm), considering composite cellular beams with PCHCS.

Table 8 – Global shear force comparative analyses between the present and previous models, considering PCHCS (in kN)

$V_{(1x300)}$	$V_{(1x450)}$	$V_{(1x450)}/V_{(1x300)}$	$V_{(2x300)}$	$V_{(2x450)}$	$V_{(2x450)}/V_{(2x300)}$
365.0±77.8	358.2±71.0	0.98	414.9±84.7	398.1±82.7	0.96

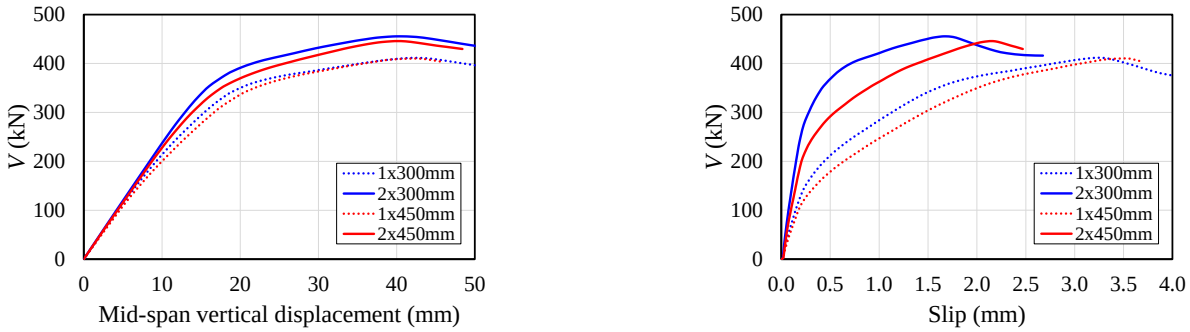

(a) Global shear force vs. mid-span vertical displacement (b) Global shear force vs. slip

Fig. 16: D_o/d=0.9 and p/D_o=1.5 models with PCHCS. Failure mode: WPB+PM

The differences between the average values of the global shear force tend to decrease, due to the failure mode being accompanied by the shear stud rupture. Another important observation was related to the ductile behavior at the interface between the PCHCS and the cellular beam. It was observed that the average slip value was 3.2±0.5mm, for the model in which there was a smaller number of connectors (1x450mm). According to EC4 [18], in order to characterize the ductile behavior at the interface, there must be a minimum 6mm of relative slip. Therefore, in all models of composite cellular beams with PCHCS analyzed so far, the behaviors at the interface were characterized as fragile.

Regarding the analyses performed on composite cellular beams with PCHCSCT, for 1x450 models, in all observations the shear stud rupture was observed. On the development of analyses, for the mid-span vertical displacement at 15.4±0.3mm (1x450mm) and 15.2±0.4mm (2x450mm), the global shear force, the von Mises stresses of tees and shear studs, and the relative slips were 269.4±35.3kN; 347.1±0.9MPa; 561.8±18.9MPa; 1.6±0.2mm and 318.3±42.9kN; 347.7±1.2MPa; 515.1.5±14.1MPa; 0.9±0.2mm for 1x450mm and 2x450mm models, respectively. With the mid-span vertical displacements at 30.1±0.5mm (1x450mm) and 30.1±1.3mm (2x450mm), the global shear force, the von Mises stresses of tees and shear studs, and the relative slips were 328.7±55.2kN; 371.8±18.5MPa; 640.7±16.6MPa; 3.0±0.3mm and 421.2±76.2kN; 380.4±24.2MPa; 603.2±21.8MPa; 2.2±0.4mm for 1x450mm and 2x450mm models, respectively. In the ultimate resistance, for the mid-span vertical displacements at 32.3±4.2mm (1x450mm) and 44.0±10.7mm (2x450mm), the global shear force, the von Mises stresses of tees and shear studs, and the relative slips were 371.1±58.6kN; 375.6±29.7MPa; 664 MPa; 3.5±0.2mm and 449.9±68.7kN; 435.7±46.5MPa; 659.1±11.4MPa; 3.1±0.4mm for 1x450mm and 2x450mm models, respectively. An example of comparations of the ultimate global shear force between the present (1x450mm and 2x450mm) and previous analyses (1x300mm and 2x300mm), considering composite cellular beams with PCHCSCT, is presented at in **Table 9** and **Fig. 17**.

Table 9 – Global shear force comparative analyses between the present and previous models with PCHCSCT (in kN)

$V_{(1x300)}$	$V_{(1x450)}$	$V_{(1x450)}/V_{(1x300)}$	$V_{(2x300)}$	$V_{(2x450)}$	$V_{(2x450)}/V_{(2x300)}$
395.9±62.0	371.1±58.6	0.94	483.7±70.7	449.9±68.7	0.93

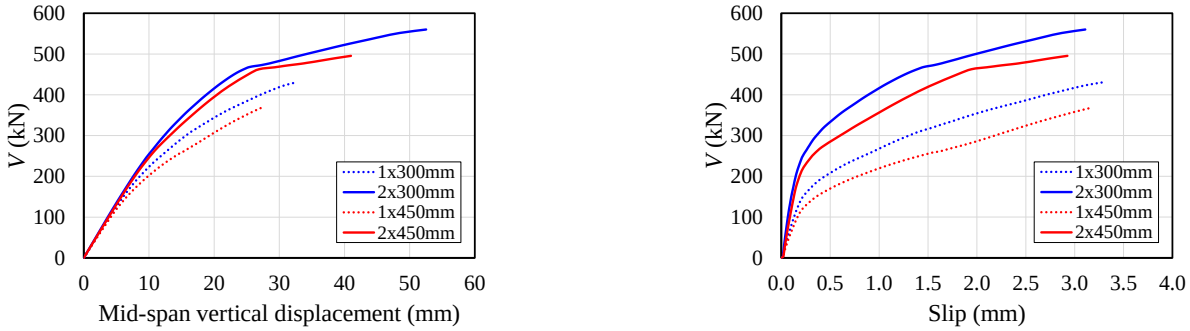

(a) Global shear force vs. mid-span vertical displacement (b) Global shear force vs. slip

Fig. 17: D_o/d=1.2 and p/D_o=1.5 models with PCHCSCT. Failure mode: VM*

Fig. 18 show the influence of the concrete topping ($V_{PCHCSCT}$-V_{PCHCS}). An important observation in p/D_o=1.5 (**Fig. 18a**) is the negative difference ($V_{PCHCSCT}$-V_{PCHCS}<0) for both 1x450mm and 2x450mm models. In the 1x450mm models the VM* was observed for both PCHCS and PCHCSCT models. For the PCHCS and PCHCSCT with 2x450mm models, the failure mode was WPB+PM* and VM*, respectively. The negative difference implies that the models with PCHCS obtained a greater global shear force compared to the models with PCHCSCT. This occurred due to the position of the neutral plastic axis. Although in the composite section with partial interaction there are two neutral plastic axes (one in cellular profile and one in the slab), in models with PCHCS, the neutral plastic axis was closer to the cellular profile. In this context, the slab will absorb a greater amount of compression stresses. On the other hand, with the presence of the concrete topping, the neutral plastic axis is closer to the compressed edge of the slab, a factor that intensifies the tensile stresses. The distance between the neutral plastic axis and the extreme fiber of the concrete slab in compression can be calculated as $nP_{sc}/0.85f_cb_{eff}$. Another observation is illustrated in **Fig. 18e**. In this illustration, for the models p/D_o=1.5 and 1x450mm, the failure modes were VM* and WPB+PM* for the models with PCHCS and PCHCSCT, respectively. In this scenario, the negative difference occurred due to the model with PCHCSCT having the resistance governed by the cellular profile. The maximum difference with a value equal to 85N was observed for the model D_o/d=0.9 and p/D_o=1.5 with 2x450mm (**Fig. 18b**). The minimum difference, which was -78kN, it was analyzed for the D_o/d=0.8 and p/D_o=1.5 model with 2x450mm (**Fig. 18a**).

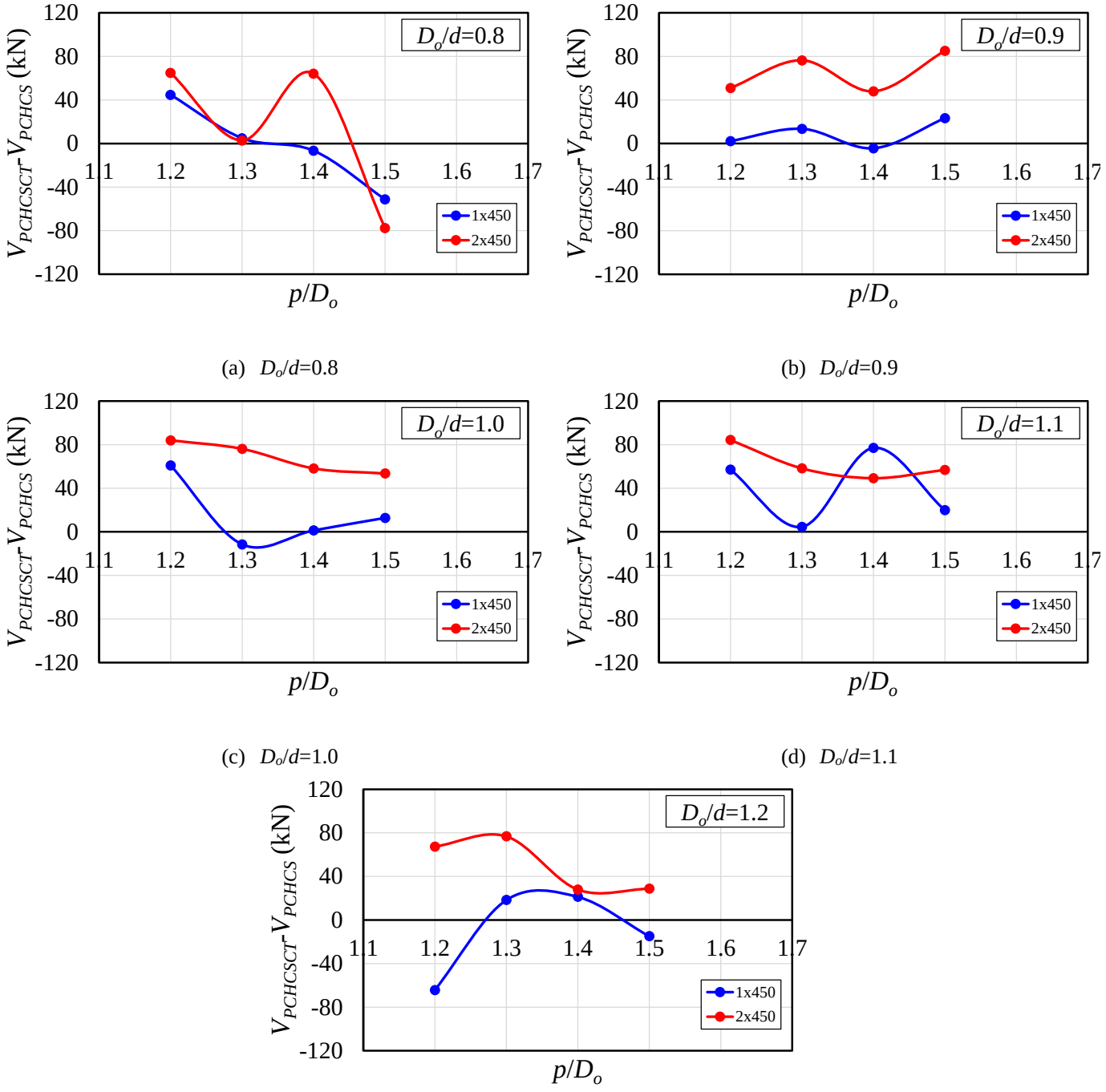

(a) D_o/d=0.8

(b) D_o/d=0.9

(c) D_o/d=1.0

(d) D_o/d=1.1

(e) D_o/d=1.2

Fig. 18: The influence of concrete topping for models with 450mm of shear studs spacing

Fig. 19 shows the shear resistance of the models analyzed as a function of key parameters, such as the D_o/d and p/D_o. It is observed that the models with 2x450mm presented greater resistance to global shear force than the models with 1x450mm. In addition, there is a drop in the resistance of the models D_o/d=1.0 and p/D_o=1.2 (**Fig 19c**), and D_o/d=1.2 and p/D_o=1.2 (**Fig 19e**), as previously presented (**Fig. 11c**, **Fig. 11e**, **Fig. 15c** and **Fig. 15e)**. Therefore, so far, it is possible to state that for all the models analyzed, double shear studs provided greater resistance than one line of shear studs. The failure modes analyzed are presented (**Table 10**).

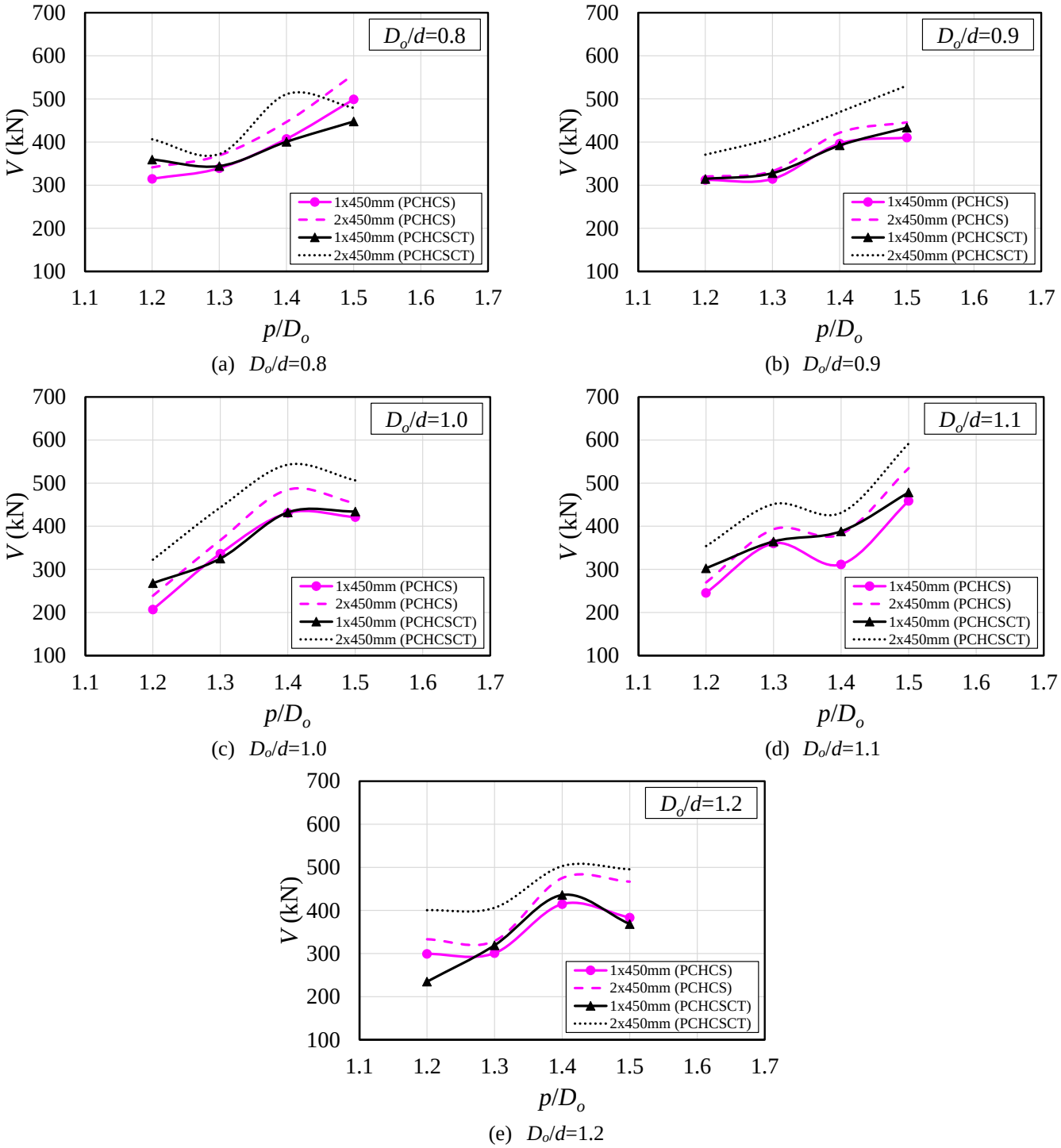

(a) D_o/d=0.8 (b) D_o/d=0.9

(c) D_o/d=1.0 (d) D_o/d=1.1

(e) D_o/d=1.2

Fig. 19: Results for models with 450mm of shear studs spacing, considering PCHCS and PCHCSCT

Table 10 – Failure modes for 1x450mm and 2x450mm models

D_o/d	p/D_o	1x450mm		2x450mm	
		PCHCSCT	PCHCS	PCHCSCT	PCHCS
0.8	1.2	VM*	VM*	WPB+PM*	VM*
	1.3	VM*	WPB+PM*	VM*	WPB+PM*
	1.4	VM*	WPB+PM*	WPB+PM*	WPB+PM
	1.5	VM*	PM*	VM*	WPB+PM
0.9	1.2	VM*	WPB+PM*	WPB+PM*	VM
	1.3	WPB+PM*	WPB+PM*	WPB+PM*	WPB+PM*
	1.4	VM*	WPB+PM*	WPB+PM*	WPB+PM*
	1.5	VM*	WPB+PM	WPB+PM*	WPB+PM
1.0	1.2	WPB+PM*	VM*	WPB+PM*	VM
	1.3	VM*	WPB+PM	WPB+PM*	WPB+PM
	1.4	VM*	WPB+PM*	VM	WPB+PM
	1.5	VM*	WPB+PM*	VM	WPB+PM*
1.1	1.2	VM*	WPB+PM	WPB+PM*	WPB+PM
	1.3	VM *	WPB+PM*	WPB+PM	WPB+PM*
	1.4	VM *	PM*	VM	WPB+PM
	1.5	VM*	VM*	VM*	VM
1.2	1.2	VM*	WPB+PM*	WPB+PM*	WPB+PM
	1.3	VM*	VM	WPB+PM*	VM
	1.4	VM*	VM*	VM*	WPB+PM
	1.5	VM*	VM*	VM*	VM

*The shear stud rupture occurred.

5.4. SUMMARY OF RESULTS

In this section the results are presented by the shear resistance of the models analyzed as a function of key parameters (D_o/d and p/D_o), considering composite cellular beams with PCHCS (**Fig. 20**) and PCHCSCT (**Fig. 21**). The illustrations are accompanied by the lateral view of the models ($L/4$ from support) to observe the shear stud position at most critical opening, which is the one that is closest to the support. It was observed in most models, that the greater the number of connectors, the greater the global shear resistance. In contrast, the smaller the number of connectors, the lower the global shear resistance. These resistance values tend to converge, since the failure mode is limited by the shear stud rupture. Another important factor regarding the number of shear studs is the equivalent resistance. For example, the resistance of the 1x150mm models was similar to the resistance of the 2x300 models. In both models, the number of shear studs is the same. Such observation was evaluated for the models with PCHCS and PCHCSCT. This statement is also valid for the 1x300mm and 2x450mm models. However, in this context, there was a small difference between the shear resistances, due to the difference between the number of shear studs, since the 1x300mm and 2x450 models have 10 and 14 shear studs (from support to mid-span), respectively. Regarding **Fig. 20a**, for the series D_o/d=0.8; p/D_o=1.3, there was a drop in resistance in the 1x300mm models compared to the 1x450mm models. This drop was also observed in **Fig. 20b** for the series D_o/d=0.9; p/D_o=1.2. This is attributed to the fact that the 1x300mm models do not have shear studs in the length of the second opening from the support, which may have caused the drop in resistance. An interesting observation presented in **Fig. 21a**, considering the series D_o/d=0.8; p/D_o=1.2-1.5 and 2x450mm, is the change in the ultimate resistance due to shear stud positioning.

For D_o/d=0.8; p/D_o=1.2;1.4, the WPB+PM* was observed, while for models D_o/d=0.8; p/Do=1.3;1.5, the VM* was observed. This is explained by the fact that the D_o/d=0.8; p/D_o=1.2;1.4 models included shear studs allocated above the first opening, unlike the D_o/d=0.8; p/Do=1.3;1.5 models, where shear studs were not allocated above the first opening. Finally, the results presented in **Fig. 20c**, **Fig. 20e**, **Fig. 21c** and **Fig. 21e** shows the pattern in the drop of resistance of the models p/Do=1.4 for the models p/Do=1.5, due to the end-post width, according to the previous discussion.

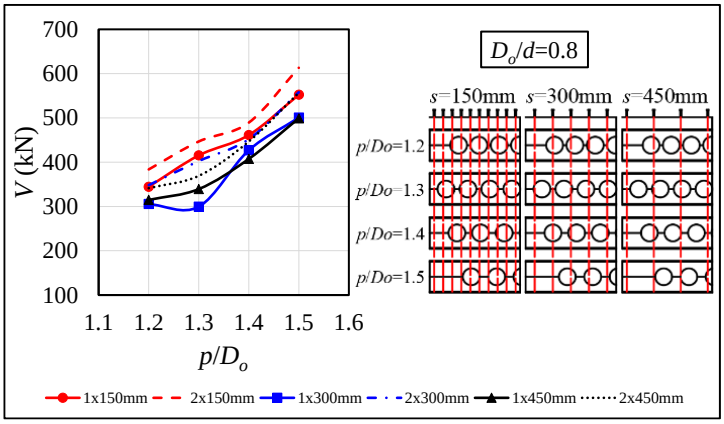

(a)D_o/d=0.8

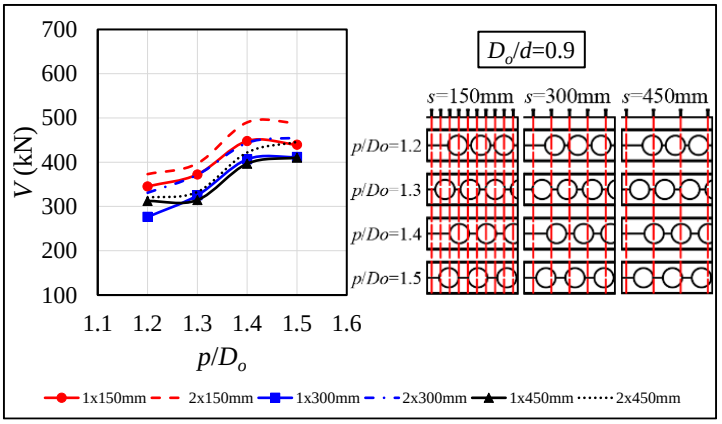

(b)D_o/d=0.9

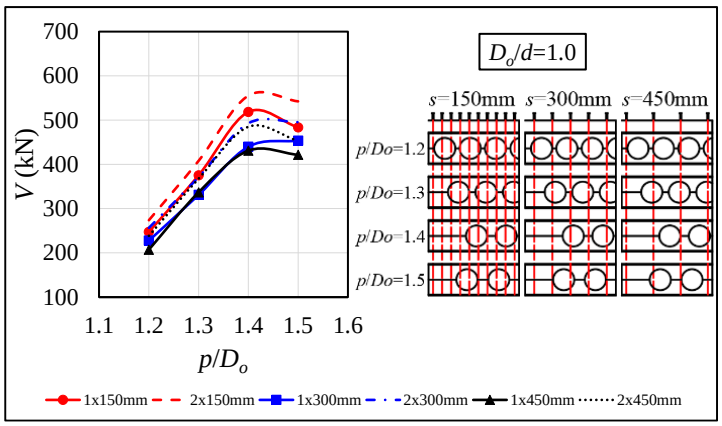

(a) D_o/d=1.0

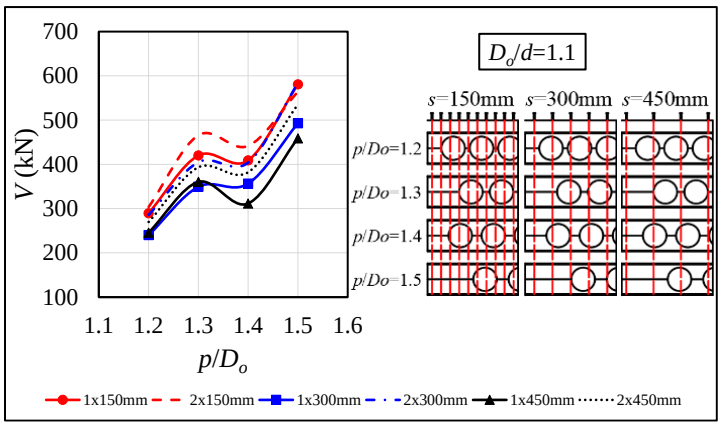

(b) D_o/d=1.1

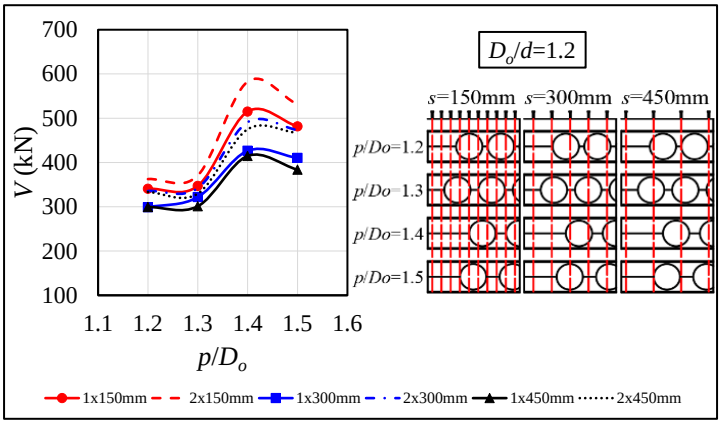

(c) D_o/d=1.2

Fig. 20: Summary of results for composite cellular beams with PCHCS

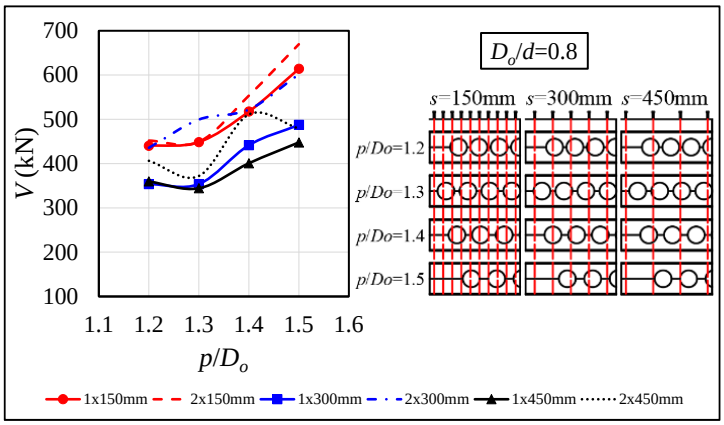

(a)D_o/d=0.8

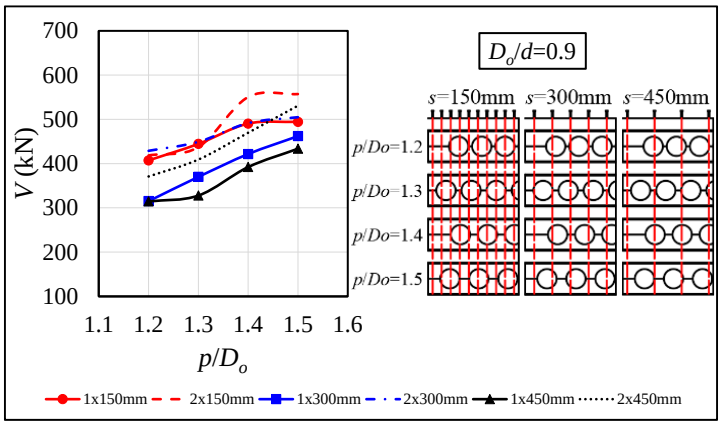

(b)D_o/d=0.9

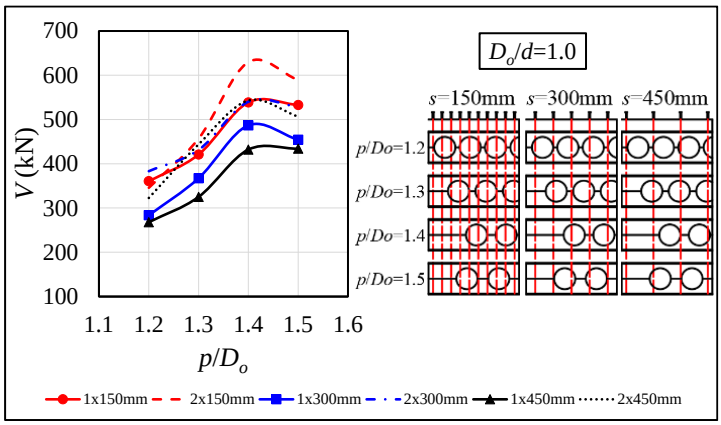

(c) D_o/d=1.0

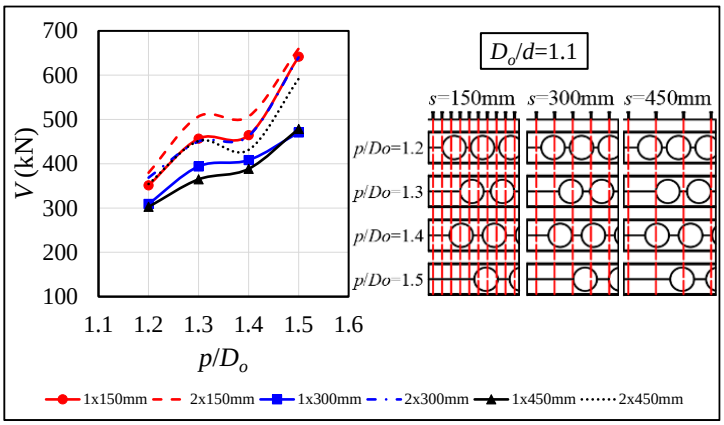

(d) D_o/d=1.1

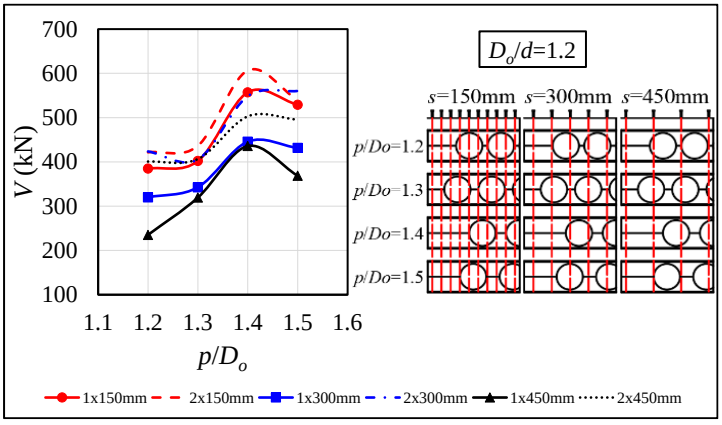

(e) D_o/d=1.2

Fig. 21: Summary of results for composite cellular beams with PCHCSCT

5.5. CALCULATION RECOMMENDATION

In this section, a calculation recommendation for WPB resistance of composite cellular beams with PCHCS or PCHCSCT is described. SCI P355 [15] presents equations for the limiting values of global shear force, considering partial (**Eq. 13**) and full interaction (**Eq. 14**). However, these equations were performed for composite beams with steel-concrete composite slabs.

$$V_{Rd} = \frac{V_{WPB}\left(D_o / p\right) + \left(4M_{bT,NV,Rd} / 0.45D_o\right)}{1 + h_{o,eff} / h_{eff}} + \frac{\Delta N_{sc,Rd}}{p}\left(y_t + h_s - 0.5h_c\right) \tag{13}$$

$$V_{Rd} = \left[V_{WPB}\left(D_o / p\right) + \left(4M_{bT,NV,Rd} / 0.45D_o\right)\right]\frac{\left(h_{eff} + h_s - 0.5h_c\right)}{h_{eff} + D_o} \tag{14}$$

The buckling resistance (V_{WPB}) is calculated according to **Eqs. (15-21)**, $M_{bT,NV,Rd}$ is the plastic resistance of the lower tee reduced due to axial tension multiplying by the approximate factor $\left[1-\left(N / N_{pl}\right)^2\right]$, and $\Delta N_{sc,Rd}$ is defined as the product of the number of connectors ($n_{sc,wp}$) in the web post width (p) by the shear studs resistance (P_{sc}).

$$\chi = \frac{1}{\phi + \sqrt{\phi^2 - \lambda_0{}^2}} \le 1.0 \tag{15}$$

$$\phi = 0.5\left[1 + \alpha\left(\lambda_0 - 0.2\right) + \lambda_0{}^2\right] \tag{16}$$

$$\lambda_0 = \sqrt{\frac{f_y}{f_{cr,w}}} \tag{17}$$

$$f_{cr,w} = \frac{\pi^2 E}{\lambda_w^2} \tag{18}$$

$$l_{eff} = 0.5\sqrt{b_w^2 + D_o^2} \le 0.7D_o \tag{19}$$

$$\lambda_w = \frac{l_{eff}\sqrt{12}}{t_w} \tag{20}$$

$$V_{WPB} = \chi f_y t_w b_w \tag{21}$$

Table 11: Imperfection factors for buckling curves according EC3

Buckling curve	*a*	*b*	*c*	*d*
Imperfection factor (α)	0.21	0.34	0.49	0.76

The SCI P355 [15] recommends using the buckling curve *c* (**Table 11**). The limits, for the use of the buckling curve *c*, are sections that have $d/b_f > 1.2$ with $40\text{mm} < t_f \le 100\text{mm}$, and $d/b_f \le 1.2$ with $t_f \le 100\text{mm}$. However, the interaction degree of composite cellular beams is not clearly defined, according to the SCI P355 [15] specifications, since this recommendation suggests choosing the lowest calculated value, between the **Eqs. (13-14)**, for the resistance prediction. Similarly, from the study by Sheehan et al. [60]

- presented in section 2, the spacing between the shear studs significantly influenced the WPB resistance. This shows that the number of shear studs must be taken into account in the resistance calculation. In addition, the combination of WPB the formation of the Vierendeel plastic hinges were verified in all models especially at the web depth of the tees.

In this context, the present study proposes a simplified way of calculating the resistant global shear force, considering composite cellular beams with PCHCS or PCHCSCT (**Eq. 22**). V_{WPB} is calculated according **Eqs. (15-21)**. $V_{pl,T}$ is the plastic shear resistance due to both tees (**Eq. 23**), taking into account two factors: (A_{wt}/A_t) and (D_o/d). This is because stating that both tees are completely plasticized can lead to overestimated results. Finally, the shear resistance due to composite action can be taken according to **Eq. (24)**:

$$V_{Rd} = V_{WPB} + V_{pl,T} + V_{VC} \tag{22}$$

$$V_{pl,T} = 4\left[\frac{A_{wT} f_y \left(0.5h_{w,T} + t_f - z_{pl}\right) + A_{fT} f_y \left(0.5t_f - z_{pl} + z_{pl}{}^2 / t_f\right)}{0.45D_o}\right]\left(\frac{A_{wT}}{A_T}\right)\left(\frac{Do}{d}\right) \tag{23}$$

$$V_{VC} = k\frac{P_{sc}}{s}\left(y_t + 0.5h_c\right) \tag{24}$$

It is not obvious which buckling curve to use, as shown in **Eq. (14)** and **Table 6**. Following, the numerical results are compared with the buckling curves *c* (**Fig. 22a**), *b* (**Fig. 22b**) and *a* (**Fig. 22c**). As it is depicted, it was observed that when only buckling resistance is considered (V_{WPB}), the resistant values tend to underestimate the shear resistance of the composite cellular beams with PCHCS and PCHCSCT. In this context, it was verified that the average values of the ratio between the analytical and numerical models (V_{FE}) are less than 65%, i.e. $V_{WPB}/V_{FE}<0.65$. These values tend to decrease as the imperfection factor (α) was increased. On the other hand, when **Eq. (20)** was considered, the average values of the ratio between the analytical and numerical models are greater than 83% ($V_{WPB}+V_{pl,T}+V_{VC}/V_{FE}>0.83$). These values tend to increase, as the imperfection factor was reduced, and this ratio can reach 94% ($V_{WPB}+V_{pl,T}+V_{VC}>0.94$) with the buckling curve *a*. In total, 142 numerical models were characterized by WPB. Considering the buckling curve *c*, only 10 observations overestimated the resistance of the models. In this context, the maximum value found for the ratio between **Eq. (20)** and the numerical model was 1.06. For buckling curves *b* and *a*, these values were increased. For the buckling curve *b*, 30 observations were overestimated, with the maximum value of the ratio at 1.14. For the buckling curve *a*, 55 observations were overestimated, with the maximum value of the ratio at 1.23. Therefore, the buckling curve *c*, as recommended by SCI P355 [15] is a good option.

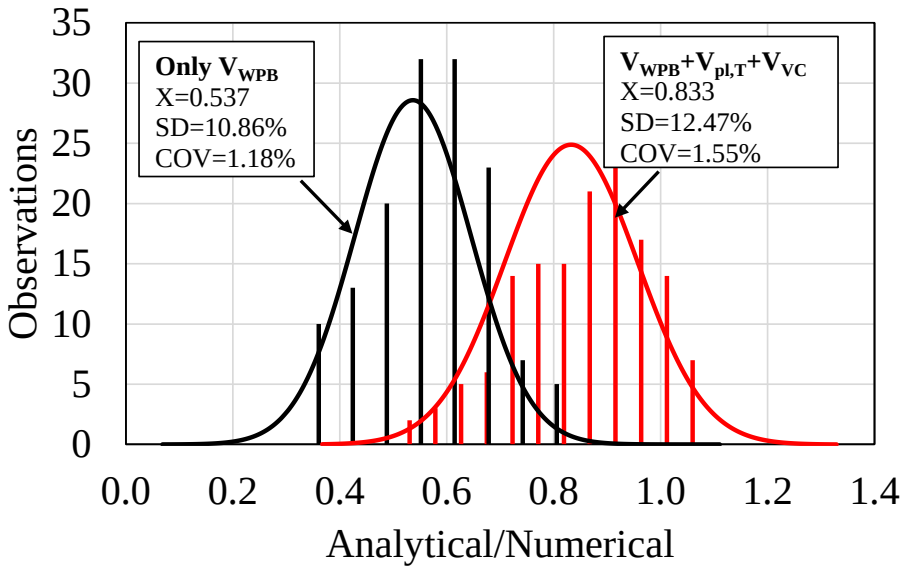

(a) V_{WPB} vs. $V_{WPB}+V_{pl,T}+V_{VC}$, considering bucking curve *c*

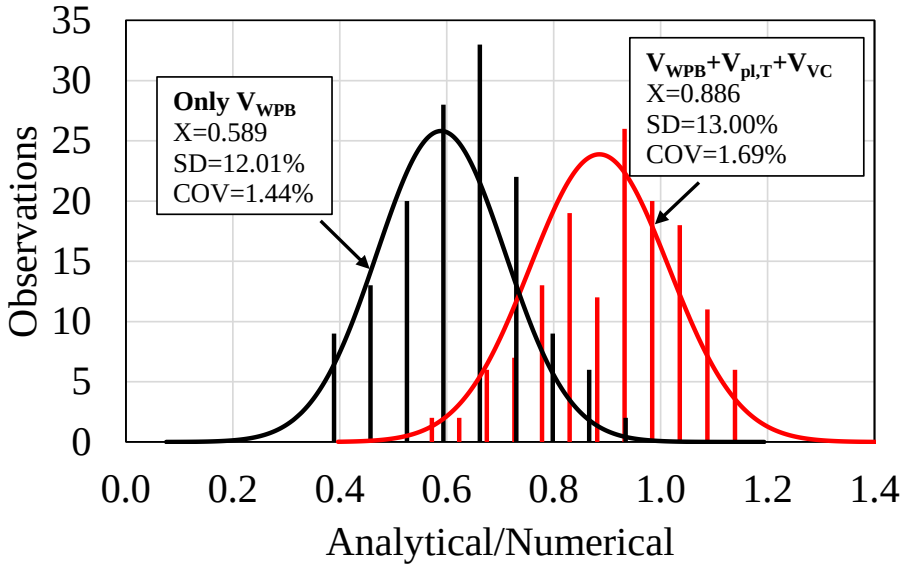

(b) V_{WPB} vs. $V_{WPB}+V_{pl,T}+V_{VC}$, considering bucking curve *b*

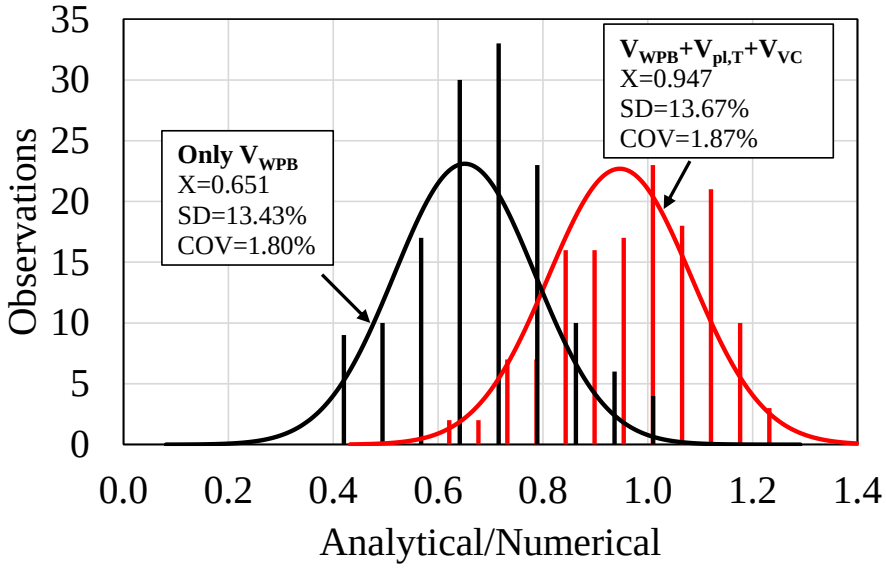

(c) V_{WPB} vs. $V_{WPB}+V_{pl,T}+V_{VC}$, considering bucking curve *a*

542 **Fig. 22: Statistical analyses**

CONCLUDING REMARKS

This paper developed a parametric study to investigate the composite action on the web post buckling resistance of composite cellular beams with PCHSC and PCHSCT. In this study, the opening diameter, the web post width and the shear studs spacing, with single and double row, were the parameters evaluated. The results of 240 models were presented and discussed. A proposed global shear resistance calculation approach of composite cellular beams with PCHCS and PCHCSCT was compared with the numerical results. It was concluded that:

1. The predominant failure mode was the combination of web post buckling with plastic mechanism. As the spacing between the shear studs was increased, that is, the number of connectors was reduced, this combination was accompanied by the shear stud rupture.
2. The shear stud rupture was observed, mainly for the analyses with PCHCSCT. In these models, the CT provided an increase in the axial resistance of the PCHCS, a factor that limited the resistance of the composite cellular beams to the resistance of the connection.
3. PCHCSCT models showed greater (or similar) global shear resistance than the PCHCS models. The CT contributed to the increase in global shear resistance. However, as the number of shear studs decreased, the resistance was similar due to the shear stud rupture. This showed that the resistance of the structural system was limited to the resistance of the connection, as the condition of partial interaction.
4. The models with two rows of shear stud presented greater global shear resistance than the models with a single row. This is due to the fact that the greater the number of connectors, the greater the resistance of the composite action. The global shear resistance was similar for the models that the shear stud rupture occurred;
5. Equivalent resistance of composite cellular beams has been verified. The models that presented the same number of shear studs, regardless of the spacing, obtained similar global shear resistance. As presented in the results summary section, the resistance of the 1x150mm models was similar to the resistance of the 2x300 models, and it is also valid for the 1x300mm and 2x450mm models. In both models that were compared, the number of shear studs is the same. This implies that the number of connectors influenced the behavior of the ultimate resistance. Therefore, the number of connectors is an important factor to be considered when calculating resistance.
6. There was a drop in global shear resistance due to the absence of shear studs in the openings close to the support. This was due to the absence of composite action. It is recommended to place shear studs above the openings next to the support, regardless of the spacing between the shear studs.
7. Ductile behavior at the connection interface was not observed in any model. This is because the relative slips greater than or equal to 6mm were not verified in any model. Therefore, even if it further reduces the number of connectors for ductile behavior to occur, it is likely that the connection will fail before reaching the acceptable slip value, which defines ductile behavior.

8. The composite action resistance is an important factor to be considered in the web post buckling resistance calculation. This means that the greater the number of shear studs, the greater the web post buckling resistance;

ACKNOWLEDGMENTS

The authors would like to thank Construção Metálica – Gerdau Aços Brasil for making available the data related to COPPETEC, PEC-18541. This work was supported by the São Paulo Research Foundation (FAPESP) [grant number #2018/22803-1].

REFERENCES

[1] Lawson RMM, Lim J, Hicks SJJ, Simms WII. Design of composite asymmetric cellular beams and beams with large web openings. J Constr Steel Res 2006;62:614–29. https://doi.org/10.1016/j.jcsr.2005.09.012.

[2] Lawson RM, Saverirajan AHA. Simplified elasto-plastic analysis of composite beams and cellular beams to Eurocode 4. J Constr Steel Res 2011;67:1426–34. https://doi.org/10.1016/j.jcsr.2011.03.016.

[3] Ahmed IM, Tsavdaridis KD. The evolution of composite flooring systems: applications, testing, modelling and eurocode design approaches. J Constr Steel Res 2019;155:286–300. https://doi.org/10.1016/j.jcsr.2019.01.007.

[4] Baran E. Effects of cast-in-place concrete topping on flexural response of precast concrete hollow-core slabs. Eng Struct 2015;98:109–17. https://doi.org/10.1016/j.engstruct.2015.04.017.

[5] Ibrahim IS, Elliott KS, Abdullah R, Kueh ABH, Sarbini NN. Experimental study on the shear behaviour of precast concrete hollow core slabs with concrete topping. Eng Struct 2016;125:80–90. https://doi.org/10.1016/j.engstruct.2016.06.005.

[6] Ferreira FPV, Martins CH, De Nardin S. Assessment of web post buckling resistance in steel-concrete composite cellular beams. Thin-Walled Struct 2021;158:106969. https://doi.org/10.1016/j.tws.2020.106969.

[7] Panedpojaman P, Thepchatri T, Limkatanyu S. Novel simplified equations for Vierendeel design of beams with (elongated) circular openings. J Constr Steel Res 2015;112:10–21. https://doi.org/10.1016/j.jcsr.2015.04.007.

[8] Tsavdaridis KD, D'Mello C. Web buckling study of the behaviour and strength of perforated steel beams with different novel web opening shapes. J Constr Steel Res 2011;67:1605–20. https://doi.org/10.1016/j.jcsr.2011.04.004.

[9] Erdal F, Saka MP. Ultimate load carrying capacity of optimally designed steel cellular beams. J Constr Steel Res 2013;80:355–68. https://doi.org/10.1016/j.jcsr.2012.10.007.

[10] Grilo LF, Fakury RH, Castro e Silva ALR de, Veríssimo G de S. Design procedure for the web-post buckling of steel cellular beams. J Constr Steel Res 2018;148:525–41. https://doi.org/10.1016/j.jcsr.2018.06.020.

[11] Kerdal D, Nethercot DA. Failure modes for castellated beams. J Constr Steel Res 1984;4:295–315. https://doi.org/10.1016/0143-974X(84)90004-X.

[12] Tsavdaridis KD, D'Mello C. Vierendeel Bending Study of Perforated Steel Beams with Various Novel Web Opening Shapes through Nonlinear Finite-Element Analyses. J Struct Eng 2012;138:1214–30. https://doi.org/10.1061/(asce)st.1943-541x.0000562.

[13] Chung KF, Liu TCH, Ko ACH. Investigation on vierendeel mechanism in steel beams with circular web openings. J Constr Steel Res 2001;57:467–90. https://doi.org/10.1016/S0143-974X(00)00035-3.

[14] Redwood R, Cho SH. Design of steel and composite beams with web openings. J Constr Steel Res 1993;25:23–41. https://doi.org/10.1016/0143-974X(93)90050-3.

[15] Lawson RM, Hicks SJ. Design of composite beams with large web openings. SCI P355. The Steel Construction Institute; 2011.

[16] Araújo DL, Sales MWR, Paulo SM, El Debs ALHC. Headed steel stud connectors for composite steel beams with precast hollow-core slabs with structural topping. Eng Struct 2016;107:135–50. https://doi.org/10.1016/j.engstruct.2015.10.050.

[17] Fares SS, Coulson J, Dinehart DW. AISC Steel Design Guide 31: Castellated and Cellular Beam Design. American Institute of Steel Construction; 2016.

[18] European committee for standardization. EN 1994-1-1: Eurocode 4 – Design of composite steel and concrete structures – Part 1-1: General rules for buildings. 2004.

[19] American Institute of Steel Construction. ANSI/AISC 360-16 - Specification for structural steel buildings. 2016.

[20] Vassart O, Hawer M, Simms I, Zhao B, Franssen JM, Nadjai A. European Commission. EUR 25122 Fire resistance of long span cellular beam made of rolled profiles. Luxemb Publ Off Eur Union 2012. https://doi.org/10.2777/38158.

[21] Verweij JG. Cellular beam-columns in portal frame structures. 2010. M.Sc. thesis. Delft University of Technology Civil Engineering, 2010.

[22] Bitar D, Demarco T, Martin P-O. Steel and composite cellular beams - Novel approach for design based on experimental studies and numerical investigations. 4th; Eur. Conf. Steel Compos. Struct. Eurosteel 2005, vol. b, Maastricht, Netherlands: Druck und Veragshaus,; ; n.d., p. 1.10-1.

[23] European committee for standardization. Eurocode 3: Design of steel structures—Part 1-1: General rules and rules for buildings 2005.

[24] ArcelorMittal. ACB® and Angelina® beams - A New Generation of Cellular Beams 2018.

[25] Redwood RG, Poumbouras G. Tests of composite beams with web holes. Can J Civ Eng 1983;10:713–21. https://doi.org/10.1139/l83-100.

[26] Redwood RG, Poumbouras G. Analysis of composite beams with web openings. J Struct Eng 1984;110:1949–58. https://doi.org/10.1061/(ASCE)0733-9445(1984)110:9(1949).

[27] Donahey RC, Darwin D. Web openings in composite beams with ribbed slabs. J Struct Eng 1988;114:518–34. https://doi.org/10.1061/(ASCE)0733-9445(1988)114:3(518).

[28] Cho SH, Redwood RG. Slab behavior in composite beams at openings. I: analysis. J Struct Eng 1992;118:2287–303. https://doi.org/10.1061/(ASCE)0733-9445(1992)118:9(2287).

[29] Cho SH, Redwood RG. Slab behavior in composite beams at openings. II: tests and verification. J Struct Eng 1992;118:2304–22. https://doi.org/10.1061/(ASCE)0733-9445(1992)118:9(2304).

[30] Ferreira FPV, Tsavdaridis KD, Martins CH, De Nardin S. Ultimate strength prediction of steel–concrete composite cellular beams with PCHCS. Eng Struct 2021;236:112082. https://doi.org/10.1016/j.engstruct.2021.112082.

[31] Lam D. Composite steel beams using precast concrete hollow core floor slabs. 1998. Ph.D. thesis. University of Nottingham, 1998.

[32] Ellobody E, Lam D. Modelling of headed stud in steel-precast composite beams. Steel Compos Struct 2002;2:355–78. https://doi.org/10.12989/scs.2002.2.5.355.

[33] Lam D. Capacities of headed stud shear connectors in composite steel beams with precast hollowcore slabs. J Constr Steel Res 2007;63:1160–74. https://doi.org/10.1016/j.jcsr.2006.11.012.

[34] Lam D. Designing composite beams with precast hollowcore slabs to Eurocode 4. Adv Steel Constr 2007;3:594–606. https://doi.org/10.18057/IJASC.2007.3.2.

[35] Lam D, Elliott KS, Nethercot DA. Experiments on composite steel beams with precast concrete hollow core floor slabs. Proc Inst Civ Eng - Struct Build 2000;140:127–38. https://doi.org/10.1680/stbu.2000.140.2.127.

[36] Lam D, Elliott KS, Nethercot DA. Parametric study on composite steel beams with precast concrete hollow core floor slabs. J Constr Steel Res 2000;54:283–304. https://doi.org/10.1016/S0143-974X(99)00049-8.

[37] Hicks SJ, Lawson RM. Design of composite beams using precast concrete slabs. SCI P287. The Steel Construction Institute; 2003.

[38] Gouchman GH. Design of composite beams using precast concrete slabs in accordance with EUROCODE 4. SCI P401. The Steel Construction Institute; 2014.

[39] Batista EM, Landesmann A. Análise experimental de vigas mistas de aço e concreto compostas por lajes alveolares e perfis laminados. COPPETEC, PEC-18541 2016.

[40] Ferreira FPV, Martins CH, De Nardin S. A parametric study of steel-concrete composite beams with hollow core slabs and concrete topping. Structures 2020;28:276–96. https://doi.org/10.1016/j.istruc.2020.08.045.

[41] Granade CJ. An investigation of composite beams having large rectangular openings in their webs. 1968. Partial M.Sc. thesis. University of Alabama, 1968.

[42] Clawson WC, Darwin D. Composite beams with web openings. ASCE J Struct Div 1982;108:145–62.

[43] Cho SH. An investigation on the strength of composite beams with web openings. 1982. M.Sc. thesis. Hanyang University, 1982.

[44] Narayanan R, Al-Amery RIM, Roberts TM. Shear strength of composite plate girders with rectangular web cut-outs. J Constr Steel Res 1989;12:151–66. https://doi.org/10.1016/0143-974X(89)90030-8.

[45] Roberts TM, Al-Amery RIM. Shear strength of composite plate girders with web cutouts. J Struct Eng 1991;117:1897–910. https://doi.org/10.1061/(ASCE)0733-9445(1991)117:7(1897).

[46] Todd DM, Cooper PB. Strength of composite beams with web openings. ASCE J Struct Div 1980;106:431–44.

[47] Donoghue CM. Strength of composite beams with web openings. ASCE J Struct Div 1982;108:2652–67.

[48] Clawson WC, Darwin D. Strength of composite beams at web openings. ASCE J Struct Div 1982;108:623–41.

[49] Benitez MA, Darwin D, Donahey RC. Deflections of composite beams with web openings. J Struct Eng 1998;124:1139–47. https://doi.org/10.1061/(ASCE)0733-9445(1998)124:10(1139).

[50] Chung K., Lawson R. Simplified design of composite beams with large web openings to Eurocode 4. J Constr Steel Res 2001;57:135–64. https://doi.org/10.1016/S0143-974X(00)00011-0.

[51] Redwood RG, Wong PK. Web holes in composite beams with steel deck. Can. Struct. Eng. Conf. -1982, Ontario, Toronto: Canadian Steel Construction Council; 1982, p. 1–41.

[52] Lawson RM, Chung KF, Price AM. Tests on composite beams with large web openings to justify existing design methods. Struct Enginee 1992;70:1–7.

[53] Park JW, Kim CH, Yang SC. Ultimate Strength of Ribbed Slab Composite Beams with Web Openings. J Struct Eng 2003;129:810–7. https://doi.org/10.1061/(asce)0733-9445(2003)129:6(810).

[54] Darwin D, Donahey RC. LRFD for composite beams with unreinforced web openings. J Struct Eng 1988;114:535–52. https://doi.org/10.1061/(ASCE)0733-9445(1988)114:3(535).

[55] Fahmy EH. Analysis of composite beams with rectangular web openings. J Constr Steel Res 1996;37:47–62. https://doi.org/10.1016/0143-974X(95)00022-N.

[56] Ferreira FPV, Martins CH, De Nardin S. Advances in composite beams with web openings and composite cellular beams. J Constr Steel Res 2020;172:106182. https://doi.org/10.1016/j.jcsr.2020.106182.

[57] Müller C, Hechler O, Bureau A, Bitar D, Joyeux D, Cajot LG, et al. Large web openings for service integration in composite floors. Technical Steel Research. European Comission, Contract No 7210-PR/315. Final report 2006.

[58] Nadjai A. Performance of cellular composite floor beams at ambient temperature. 2005.

[59] Nadjai A, Vassart O, Ali F, Talamona D, Allam A, Hawes M. Performance of cellular composite floor beams at elevated temperatures. Fire Saf J 2007;42:489–97. https://doi.org/10.1016/j.firesaf.2007.05.001.

[60] Sheehan T, Dai X, Lam D, Aggelopoulos E, Lawson M, Obiala R. Experimental study on long spanning composite cellular beam under flexure and shear. J Constr Steel Res 2016;116:40–54. https://doi.org/10.1016/j.jcsr.2015.08.047.

[61] Ferreira FPV, Tsavdaridis KD, Martins CH, De Nardin S. Buckling and post-buckling analyses of composite cellular beams. Compos Struct 2021;262:113616. https://doi.org/10.1016/j.compstruct.2021.113616.

[62] El-Lobody E, Lam D. Finite Element Analysis of Steel-Concrete Composite Girders. Adv Struct Eng 2003;6:267–81. https://doi.org/10.1260/136943303322771655.

[63] European committee for standardization. Eurocode 2: Design of concrete structures - Part 1-1 : General rules and rules for buildings 2004.

[64] Ferreira FPV, Rossi A, Martins CH. Lateral-torsional buckling of cellular beams according to the possible updating of EC3. J Constr Steel Res 2019;153:222–42. https://doi.org/10.1016/j.jcsr.2018.10.011.

[65] Ferreira FPV, Martins CH. LRFD for Lateral-Torsional Buckling Resistance of Cellular Beams. Int J Civ Eng 2020;18:303–23. https://doi.org/10.1007/s40999-019-00474-7.

[66] Rossi A, Ferreira FPV, Martins CH, Mesacasa Júnior EC. Assessment of lateral distortional buckling resistance in welded I-beams. J Constr Steel Res 2020;166:105924. https://doi.org/10.1016/j.jcsr.2019.105924.

[67] Rajana K, Tsavdaridis KD, Koltsakis E. Elastic and inelastic buckling of steel cellular beams under strong-axis bending. Thin-Walled Struct 2020;156:106955. https://doi.org/10.1016/j.tws.2020.106955.

[68] Ellobody E. Nonlinear analysis of cellular steel beams under combined buckling modes. Thin-Walled Struct 2012;52:66–79. https://doi.org/10.1016/j.tws.2011.12.009.

[69] Dassault Systèmes Simulia. Abaqus 6.18 2016.

[70] Chen S, Jia Y. Numerical investigation of inelastic buckling of steel–concrete composite beams prestressed with external tendons. Thin-Walled Struct 2010;48:233–42. https://doi.org/10.1016/j.tws.2009.10.009.

[71] Zhou W-B, Yan W-J. Refined nonlinear finite element modelling towards ultimate bending moment calculation for concrete composite beams under negative moment. Thin-Walled Struct 2017;116:201–11. https://doi.org/10.1016/j.tws.2017.02.011.

[72] Hillerborg A, Modéer M, Petersson P-E. Analysis of crack formation and crack growth in concrete by means of fracture mechanics and finite elements. Cem Concr Res 1976;6:773–81. https://doi.org/10.1016/0008-8846(76)90007-7.

[73] Lubliner J, Oliver J, Oller S, Oñate E. A plastic-damage model for concrete. Int J Solids Struct 1989;25:299–326. https://doi.org/10.1016/0020-7683(89)90050-4.

[74] Lee J, Fenves GL. Plastic-Damage Model for Cyclic Loading of Concrete Structures. J Eng Mech 1998;124:892–900. https://doi.org/10.1061/(ASCE)0733-9399(1998)124:8(892).

[75] Yu T, Teng JG, Wong YL, Dong SL. Finite element modeling of confined concrete-I: Drucker–Prager type plasticity model. Eng Struct 2010;32:665–79. https://doi.org/10.1016/j.engstruct.2009.11.014.

[76] Carreira DJ, Chu KH. Stress-Strain Relationship for Plain Concrete in Compression. ACI J Proc 1985;82:797–804. https://doi.org/10.14359/10390.

[77] Carreira DJ, Chu KH. Stress-Strain Relatonship for Reinforced Concrete in Tension. J Am Concr Inst 1986;83:21–8.

[78] Behnam H, Kuang JS, Samali B. Parametric finite element analysis of RC wide beam-column connections. Comput Struct 2018;205:28–44. https://doi.org/10.1016/j.compstruc.2018.04.004.

[79] Genikomsou AS, Polak MA. Finite element analysis of punching shear of concrete slabs using damaged plasticity model in ABAQUS. Eng Struct 2015;98:38–48. https://doi.org/10.1016/j.engstruct.2015.04.016.

[80] Ferreira FPV, Martins CH, De Nardin S. Sensitivity Analysis of Composite Cellular Beams to Constitutive Material Models and Concrete Fracture. Int J Struct Stab Dyn 2021;21:2150008. https://doi.org/10.1142/S0219455421500085.

[81] Ferreira FPV, Tsavdaridis KD, Martins CH, De Nardin S. Steel–Concrete-Composite Beams with Precast Hollow-Core Slabs: A Sustainable Solution. Sustainability 2021;13:4230. https://doi.org/10.3390/su13084230.

[82] Nguyen TNH, Tan KH, Kanda T. Investigations on web-shear behavior of deep precast, prestressed concrete hollow core slabs. Eng Struct 2019;183:579–93. https://doi.org/10.1016/j.engstruct.2018.12.052.

[83] Yun X, Gardner L. Stress-strain curves for hot-rolled steels. J Constr Steel Res 2017;133:36–46. https://doi.org/10.1016/j.jcsr.2017.01.024.

[84] Elharouney O, Elkateb M, Khalil A. Behaviour of prestressed hollow core slabs strengthened with NSM CFRP strips around openings: A finite element investigation. Eng Struct 2021;238:112262. https://doi.org/10.1016/j.engstruct.2021.112262.

[85] Nguyen HTN, Tan K-H. Shear response of deep precast/prestressed concrete hollow core slabs subjected to fire. Eng Struct 2021;227:111398. https://doi.org/10.1016/j.engstruct.2020.111398.

[86] Wijesiri Pathirana S, Uy B, Mirza O, Zhu X. Flexural behaviour of composite steel–concrete beams utilising blind bolt shear connectors. Eng Struct 2016;114:181–94. https://doi.org/10.1016/j.engstruct.2016.01.057.

748 [87] Katwal U, Tao Z, Hassan MK, Uy B, Lam D. Load sharing mechanism between shear studs and profiled steel sheeting in
749 push tests. J Constr Steel Res 2020;174:106279. https://doi.org/10.1016/j.jcsr.2020.106279.

750 [88] Guezouli S, Lachal A. Numerical analysis of frictional contact effects in push-out tests. Eng Struct 2012;40:39–50.
751 https://doi.org/10.1016/j.engstruct.2012.02.025.

752 [89] Sjaarda M, Porter T, West JS, Walbridge S. Fatigue Behavior of Welded Shear Studs in Precast Composite Beams. J Bridg
753 Eng 2017;22:04017089. https://doi.org/10.1061/(ASCE)BE.1943-5592.0001134.

754 [90] Liu X, Bradford MA, Chen Q-J, Ban H. Finite element modelling of steel–concrete composite beams with high-strength
755 friction-grip bolt shear connectors. Finite Elem Anal Des 2016;108:54–65. https://doi.org/10.1016/j.finel.2015.09.004.

756